Asian and Oceanic forum for Pediatric Radiology

AOfPR

2024

22nd Annual Scientific Meeting of
Asian and Oceanic Society for Pediatric Radiology
Bali, Indonesia

September 25 - 28th, 2024

Proceeding Book — 22nd Annual Scientific Meeting of Asian and Oceanic Society for Pediatric Radiology

ARTIFICIAL INTELLIGENCE IN PEDIATRIC RADIOLOGY

September 25-28, 2024
Mövenpick Resort & Spa Jimbaran
Bali, Indonesia

Asian-Oceanic Society for Pediatric Radiology

Proceeding Book — 22nd Annual Scientific Meeting of Asian and Oceanic Society for Pediatric Radiology

ARTIFICIAL INTELLIGENCE IN PEDIATRIC RADIOLOGY

Table of Contents

FOREWORD

As the Chairman of the Asian & Oceanic Society for Pediatric Radiology (AOSPR) 2024, I am honored to present this collection of research and developments in the field of pediatric radiology. Our society has consistently enhanced pediatric imaging techniques and research throughout the Asia-Pacific region.

Pediatric radiology demands precision, care, and continuous innovation. The unique needs of our young patients require us to constantly improve imaging techniques. The work showcased in this publication provides valuable insights and solutions, paving the way for future advancements and setting new standards of excellence.

I deeply thank all contributors, authors, and reviewers for making this publication possible. Your dedication reflects the strength of our society. I also appreciate our members for their support and active participation, which are vital to our success.

As we move forward, I am confident that the AOSPR will continue to lead the way in innovation and excellence. Together, we will strive to enhance the health and well-being of children through the application of advanced imaging techniques and collaborative research.

Thank you for your unwavering commitment to our mission. I trust that this publication will serve as a valuable resource and inspiration for all professionals dedicated to the field of pediatric radiology.

Herlina Uinarni, MD

Chairman of AOSPR 2024

LOCAL FACULTY & ORGANIZING COMMITTEE

ADVISOR	Prof. Rista D. Soetikno, MD
	Adji Saptogino, MD
CHAIRMAN	Herlina Uinarni, MD
CO-CHAIRMAN	Pande Putu Yuli A, MD
SECRETARIAT	Rahmi Alfiah, MD
	Dessy Wimelda, MD
	Rafikah Rauf, MD
	Susyana
TREASURER	Jeanne Leman, MD
SCIENTIFIC PROGRAMME	Farah Hendara Ningrum, MD
	Damayanti Sekarsari, MD
	M. Yanuar Amal, MD

INTERNATIONAL FACULTY & SPEAKERS

*The list below is in alphabetical order

Ashley Robinson
Qatar

Bernard Laya
The Philippines

Beth M. Kline-Fath
USA

Claudia Cheung
Hong Kong

David Stringer
Singapore

Edward Lee
USA

Elaine Kan
Hong Kong

Faizah Mohd Zaki
Malaysia

In One Kim
Korea

Jeevesh Kapur
Singapore

Ji Hye Kim
Korea

Joanna Kasznia-Brown
UK

Joyce Chan
Hong Kong

Kiran Hilal
Pakistan

Kushaljit Singh Sodhi
India

Yu-Min (Maggie) Zhong
China

Nathan David P. Concepcion
The Philippines

Shunsuke Nosaka
Japan

Supika Kritsaneepaiboon
Thailand

Tatsuo Kono
Japan

Timothy Cain
Australia

Wendy Lam
Hong Kong

Winnie Chu
Hong Kong

LOCAL SPEAKERS & MODERATORS

*The list below is in alphabetical order

Damayanti Sekarsari

Eddy Sudijanto

Farah Hendara Ningrum

Herlina Uinarni

Indrastuti Normahayu

L. Adji Saptogino

Mohammad Yanuar Amal

Ni Nyoman Margiani

Pande Putu Yuli Anandasari

Rahmi Alfiah Nur Alam

Utami Purbasari

TOP 5 E-POSTER PRESENTATIONS

Artificial Intelligence in Pediatric Intussusception Detection: A Systematic Review and Meta-analysis

***Jessica Christanti*[1], *Ratna Sutanto*[1,2], *Jeanne Leman*[1,2]**

[1] *Radiology Department, Medical Faculty of Pelita Harapan University, Indonesia*
[2] *Radiology Department, Siloam Hospitals Lippo Village, Jakarta, Indonesia*

ARTIFICIAL INTELLIGENCE IN PEDIATRIC INTUSSUSCEPTION DETECTION: A SYSTEMATIC REVIEW AND META-ANALYSIS

Jessica Christanti[1], Ratna Sutanto[1,2], Jeanne Leman[1,2]
[1] Radiology Department, Medical Faculty of Pelita Harapan University, Indonesia
[2] Radiology Department, Siloam Hospitals Lippo Village, Jakarta, Indonesia

BACKGROUND & PURPOSE

Intussusception needs to be diagnosed immediately to prevent complications such as ischemia and intestinal perforation. It can be diagnosed by a colon in the loop, abdominal radiograph, and ultrasound, with the best accuracy on ultrasound. Artificial intelligence (AI) is expected to help radiologists and clinicians make the diagnosis.

This systematic review and meta-analysis will assess the diagnostic accuracy of AI-based radiology modalities in pediatric intussusception.

METHODS

- 8 Databases dan 1 Registry: Pubmed, Scopus, Proquest, MedRxiv, BioRxiv, SSRN, Cochrane Central, Google Scholar, and PROSPERO until June 8, 2024.
- This study already registered in PROSPERO (ID: 543569)
- The diagnostic value of AI-based radiology modalities : pooled sensitivity, specificity, positive likelihood ratio (PLR), negative likelihood ratio (NLR), diagnostic odds ratio (DOR), and area under the curve (AUC).
- Meta-analyses were performed using STATA 17.0 (Stata Corp LP, TX, USA), and Meta-DiSc 2.0 (Romany Cajal Hospital, Madrid, Spain)
- QUADAS 2 to assess the risk of bias and APPRAISE-AI to evaluate the quality of AI studies.
- Heterogeneity analysis was performed using receiver operating characteristic (ROC) and sensitivity analysis.
- The clinical utility of AI-based radiology modalities was assessed using Fagan's nomogram.

INCLUSION

- Diagnostic study design,
- Studies that include AI assessment for Intussusception,
- Human-based studies,
- Absolute numbers of true-positive, false-positive, or false negative, or true-negative could be calculated from the study.

EXCLUSION

- Non-human subject research,
- Case report/series
- Commentary/viewpoint,
- Narrative review,
- Irretrievable full-text article.

RESULT

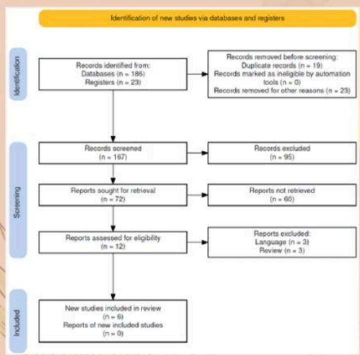

Figure 1. Preferred Reporting Items for Systematic Reviews and Meta-Analyses (PRISMA) 2020 flow chart of the study selection process

Author	Year	Imaging Modality	No. images per set			Reference Standard	TN	FP	FN	TP	Algorithm
			Training	Tuning	Testing						
Kwon et al.	2020	Abdominal Radiography	11384	11384	255	Expert consensus	4633	349	130	594	Deep convolutional neural network (CNN)
Kim et al.	2019	Abdominal Radiography	681	NR	75	Expert consensus	48	2	6	19	The You-Only-Look-Once (YOLO)v3
Xiong Chen et al.	2023	Ultrasound	6959	1927	985	Expert consensus	798	33	532	2791	Children Intussusception Diagnosis Network (CIDNet)
Zheming Li et al.	2022	Ultrasound	2325	586	142	Expert consensus	411	35	7	133	Region Convolutional Neural Network features (RCNN)
Kim et al.	2023	Ultrasound	38148	5724	2617	Expert consensus	103	1	0	20	The YOLOv5 Architecture
Pei et al.	2023	Ultrasound	6081	2023	632	Expert consensus	182	6	12	227	Modified YOLOv5

TN: True Negative, FP: False Positive, FN: False Negative, TP: True Positive
Table 1. Characteristics of AI Studies on Pediatric Intussusception

	Estimate	95% LCI	95% UCI
Sensitivity	0.901	0.823	0.947
Specificity	0.953	0.928	0.969
DOR	183.778	81.815	412.814
LR+	19.023	12.353	29.295
LR-	0.104	0.056	0.19

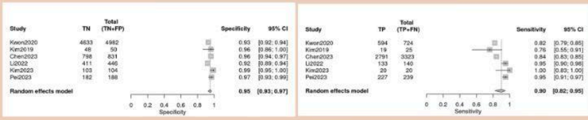

Figure 2. Forest plot of diagnostic value for Artificial Intelligence in detecting Pediatric Intussusception.

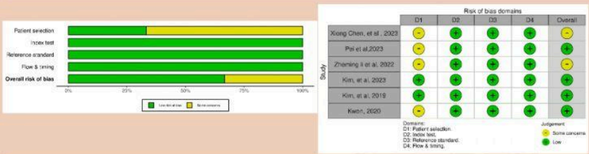

Figure 3. Quality Assessment of Included Study

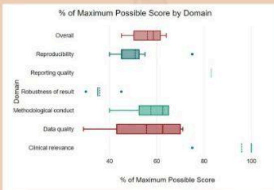

Figure 4. APPRAISE-AI Domain and Overall Scores

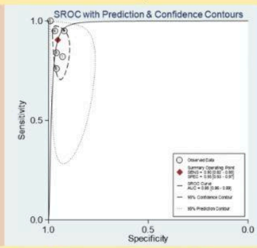

Figure 5. Summary Receiver Operating Characteristics (SROC) curve of Artificial Intelligence in detecting Pediatric Intussusception

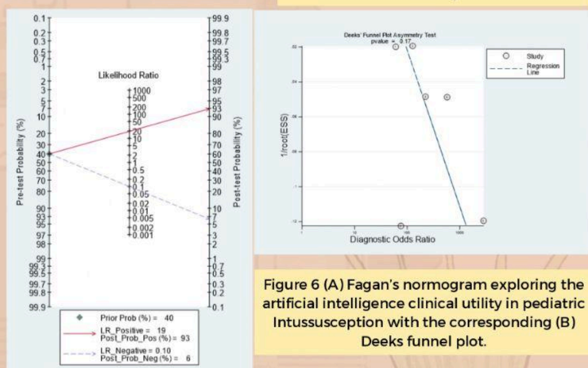

Figure 6 (A) Fagan's normogram exploring the artificial intelligence clinical utility in pediatric Intussusception with the corresponding (B) Deeks funnel plot.

CONCLUSION

AI-based ultrasound and abdominal radiograph modalities can help clinicians identify Intussusception. Korea and China are suitable populations for implementation.

REFERENCES

1. Kim S, Yoon H, Lee MJ, et al. Performance of deep learning-based algorithm for detection of ileocolic intussusception on abdominal radiographs of young children. Sci Rep; 9. Epub ahead of print 1 December 2019. DOI: 10.1038/s41598-019-55536-6.
2. Pei Y, Wang G, Cao H, et al. A deep-learning pipeline to diagnose pediatric intussusception and assess severity during ultrasound scanning: a multicenter retrospective-prospective study. NPJ Digit Med; 6. Epub ahead of print 1 December 2023. DOI: 10.1038/s41746-023-00930-8.
3. Kwong JCC, Khondker A, Lajkosz K, et al. APPRAISE-AI Tool for Quantitative Evaluation of AI Studies for Clinical Decision Support. JAMA Netw Open. Epub ahead of print 2023. DOI: 10.1001/jamanetworkopen.2023.35377.
4. Wiyarta E, Nugraha DA, Ramadani MI, et al. Clinical utility and diagnostic value of tumor-educated platelets in lung cancer: a systematic review and meta-analysis. Frontiers in Oncology; 13. Epub ahead of print 2023. DOI: 10.3389/fonc.2023.1201713.
5. Chen X, You G, Chen Q, et al. Development and evaluation of an artificial intelligence system for children intussusception diagnosis using ultrasound images. iScience; 26. Epub ahead of print 21 April 2023. DOI: 10.1016/j.isci.2023.106456.
6. Li Z, Song C, Huang J, et al. Performance of Deep Learning-Based Algorithm for Detection of Pediatric Intussusception on Abdominal Ultrasound Images. Gastroenterol Res Pract; 2022. Epub ahead of print 2022. DOI: 10.1155/2022/9285238.
7. Kwon G, Ryu J, Oh J, et al. Deep learning algorithms for detecting and visualising intussusception on plain abdominal radiography in children: a retrospective multicenter study. Sci Rep; 10. Epub ahead of print 1 December 2020. DOI: 10.1038/s41598-020-74653-1.
8. Kim SW, Cheon JE, Choi YH, et al. Feasibility of a deep learning artificial intelligence model for the diagnosis of pediatric ileocolic intussusception with grayscale ultrasonography. Ultrasonography 2024; 43: 57-67.

High-pitch Photon-counting CT of the Trunk for Small Children

Tetsu Niwa

Department of Diagnostic Radiology, Tokai University School of Medicine

High-pitch photon-counting CT of the trunk for small children

Tetsu Niwa, MD, PhD, Department of Diagnostic Radiology, Tokai University School of Medicine

Background: Recently introduced photon-counting computed tomography (CT) features a new detector system, which directly convert X-ray photons to electrical signals, thereby providing high image quality. The clinically available photon-counting CT has dual-source systems that enable rapid scanning, which could be beneficial for scanning small children to reduce motion artifacts. However, image quality of high-pitch PCCT for small children is not well understood.

Purpose: The aim of this study was to assess the image quality of PCCT using high-pitch image acquisition for the trunk of small children.

Methods: PCCT images obtained with high-pitch image acquisition for 54 children under 5 years old were retrospectively assessed. CT images with a thickness of 1 mm were evaluated in terms of visibility of the lung, abdominal major organs, and great vessels, artifact, noise, and overall image quality were rated by a broad-certified radiologist on a 5-point scale (1=non-diagnostic; 5=excellent). The visibility of the grate vessels was only assessed on contrast-enhanced CT. Volume CT dose index (CTDIvol) of each CT examination was recorded.

Results: This study included 20 non-contrast CT and 34 contrast-enhanced CT examinations. Mean pitch used was 2.4 (range, 2.0–3.0). Mean score (range) for visibility of the lung and abdominal organs, great vessels, artifact, and noise were 4.6 (3–5), 4.1 (3–5), 4.5 (4–5), 4.4 (3–5), and 4.1 (3–5), respectively. Mean score (range) for overall image quality was 4.3 (3–5). Mean CTDIvol was 1.71 ± 0.22 mGy.

Conclusion: High-pitch PCCT generally provides good image quality for the trunk of small children.

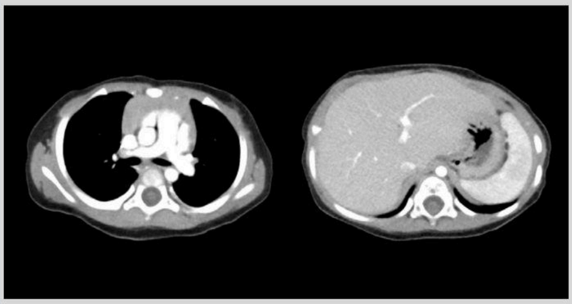

9-month-old, inspiratory stridor
BW 7.3 kg
Pitch = 2.7
Acquisition time ≒ 0.5 s
CTDIvol 1.9 mGy

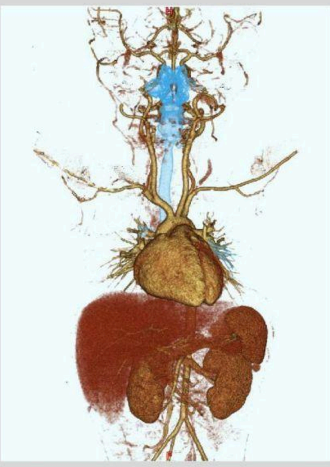

References

1. Flohr T, et al. Photon-counting CT review. Phys Med. 2020;79:126-36.

2. Leng S, et al. Photon-counting detector CT: system design and clinical applications of an emerging technology. Radiographics. 2019;39(3):729-43.

MR Features in Advanced Retinoblastoma - What a Paediatric Radiologist Needs to Know

L Ching[1], KFK Fung[2], ES Wong[3], JC Yam[3], YLE Kan[2]

[1] Department of Diagnostic and Interventional Radiology, Queen Elizabeth Hospital, Hong Kong SAR
[2] Department of Radiology, Hong Kong Children's Hospital, Hong Kong SAR
[3] Department of Ophthalmology and Visual Sciences, Chinese University of Hong Kong, Hong Kong SAR

MR Features in Advanced Retinoblastoma – What a Paediatric Radiologist Needs to Know

L Ching[1], KFK Fung[2], ES Wong[3], JC Yam[3], YLE Kan[2]
[1]Department of Diagnostic and Interventional Radiology, Queen Elizabeth Hospital, Hong Kong SAR
[2]Department of Radiology, Hong Kong Children's Hospital, Hong Kong SAR
[3]Department of Ophthalmology and Visual Sciences, Chinese University of Hong Kong, Hong Kong SAR

伊利沙伯醫院 QUEEN ELIZABETH HOSPITAL

香港兒童醫院 Hong Kong Children's Hospital

Introduction

- Retinoblastoma is the most common intra-ocular malignancy in children worldwide, with an estimated incidence of 1 per 18,000-30,000 live births.
- Precise identification of these features and accurate staging are important for oncologists and interventional radiologists to formulate the treatment plan and estimate the prognosis for parental counselling.

Retinoblastoma Staging

- According to the current retinoblastoma staging systems, there are multiple features indicating advanced disease.
- Current treatment modalities include focal therapy such as laser or cryotherapy, intravenous chemo-therapy, intra-arterial chemotherapy and surgical enucleation. Focal therapy is proven to be effective only in relatively early stage disease.
- For advanced stage disease, surgical enucleation, neoadjuvant and adjuvant systemic chemotherapy are recommended to reduce the recurrence rate and improve the overall survival.
- However, surgical enucleation is well known to impose significant side effect on patient's daily life, in particular permanent loss of vision in one eye.
- Therefore, accurate staging, in particular correctly recognizing the features indicative of high grade disease, is essential to avoid unnecessary or delay the indicated vision-losing surgery and adjuvant therapy.

AJCC Clinical Staging 8th edition, 2017	ICRB group Shields, 2006	Recommended treatment
cT1 Intra-retinal tumour(s) with subretinal fluid ≤5 mm from base of any tumour cT1a Tumours ≤3 mm and further than 1.5 mm from disc and fovea cT1b Tumours >3 mm or closer than 1.5 mm from disc or fovea	A, > 3mm to fovea or B, 1.5 to 3 mm B, ≤3 mm or C, 3 to 5 mm	For ICRB group A or B: • laser coagulation • Thermotherapy • Cryotherapy • Brachytherapy
cT2 Intraocular tumour(s) with retinal detachment, vitreous seeding, or subretinal seeding cT2a Subretinal fluid >5 mm from the base of any tumour cT2b Vitreous seeding and/or subretinal seeding	C, or E, tumour >50% of eye volume C, ≤3 mm or D, > 3 mm or E, tumour >50% of eye volume	For ICRB group C: • Systemic chemotherapy • Intra-arterial chemotherapy • Intra-vitreal chemotherapy
cT3 Advanced intraocular tumour(s) cT3a Phthisis or pre-phthisis bulbi cT3b Tumour invasion of choroid, pars plana, ciliary body, lens, zonules, iris, or anterior chamber cT3c Raised intraocular pressure with neovascularization and/or buphthalmos cT3d Hyphaema and/or massive vitreous haemorrhage cT3e Aseptic orbital cellulitis	E E E E E	For ICRB group D or E: • Systemic chemotherapy • Intra-arterial chemotherapy • Intra-vitreal chemotherapy • Enucleation • Adjuvant systemic chemotherapy in selected high risk cases
cT4 Extraocular tumour(s) involving orbit, including optic nerve cT4a Radiologic evidence of retrobulbar optic nerve involvement or thickening of optic nerve or involvement of orbital tissues cT4b Extraocular tumour clinically evident with proptosis and/or an orbital mass		

Table 1: the American Joint Committee on Cancer (AJCC) Clinical Staging 8th edition and the International Classification for Intraocular Retinoblastoma (ICRB) and the recommended treatment

Retinal Detachment

- Under MRI, retinal detachment is characterised by T2-weighted hypointense line which limited anteriorly by the ora serrata, and posteriorly converge on the optic disc

Figure 1: The axial (left) and sagittal (right) MRI T1-weighted images of a 23-month-old boy having retinoblastoma in both eyes. In left eye, there is T1-weighted hypointense retinoblastoma, with adjacent V-shaped T1-weighted hyperintense subretinal tissue converging to the optic disc (white arrow), which is signature for retinal detachment.

Vitreous and subretinal seeding

- Characterised by small foci of signal that is similar as the primary tumour in the background of the T2 hyperintense vitreous or along the retina.
- Gold standard of detecting seeding is by fundus photography, and the absence of seeding at MRI cannot exclude the presence of seeding due to the small size.

Figure 2 (left) Axial T2-weighted MRI image and (right) axial T1-weighted post-contrast image of a 2-month-old girl with retinoblastoma in both eyes. There is a T2 hypointense focus (arrow) with contrast enhancement (curved arrow) on the medial aspect of right retina, which is suggestive of subretinal seeding.

Choroid invasion

- The choroid is a highly vascular layer underneath and supports the metabolism of retina, and this predisposes the patient to distal metastasis and all-call mortality when it is invaded.
- Traditionally, enucleation of the globe is recommended for retinoblastoma patient with choroid invasion, but recently more and more case reports have shown the success of systemic and intra-arterial chemotherapy in disease control.
- Massive choroidal invasion more than 3mm in post enucleation histopathology indicates high risk disease and warrants the use of adjuvant chemotherapy to reduce the risk of metastasis.
- At MRI, choroid invasion is shown by the discontinuation of the enhancing choroid layer.

Figure 3 Axial T1-weighted post-contrast MRI images of a 40-day-old girl with left eye retinoblastoma. There is mural defect in the posterior aspect (arrow) and lateral aspect (curved arrow) of the choroid layer of left globe, suggestive of invasion. Noted there is also aseptic orbital cellulitis in the left globe, which is another imaging feature indication of high grade retinoblastoma.

Anterior segment invasion and increase intra-ocular pressure

- Together with increased inflammation in the anterior chamber and direct reduction of its volume, it is common to have elevated intra-ocular pressure at the same time.
- Under MRI, anterior segment invasion is shown by loss of normal plane between the tumour and the anterior chamber structure, in particular the lens and the ciliary body.
- Increase in intra-ocular pressure has to be suspected when there is increase in globe size or reduction of anterior chamber depth

Figure 4 (left) Oblique sagittal T2-weighted MRI image and (right) axial T2-weighted MRI image of a 19-month-old patient with right eye retinoblastoma. The large tumour in posterior aspect of right globe is inseparable with the ciliary body and lens of right eye (arrow), indicative of anterior chamber invasion. The anterior chamber depth of right eye is reduced, which is suggestive of underlying raised intraocular pressure.

Iris neovascularisation

- It is hypothesized that the increase in vascularity can reduce drainage by the lymphatic system secondary to the mass effect of retinoblastoma, promoting the vascular endothelial growth factor release.
- The leaky new vessels allow contrast leakage, shown by increased enhancement in the anterior chamber

Figure 5 (left) Axial image of T1-weighted post contrast MRI image. (right) Oblique sagittal T1-weighted post-contrast MRI image of the left eye of a 13-month-old boy with retinoblastoma. Increase in contrast enhancement of the anterior chamber is seen in left eye when comparing with the normal right eye (arrow).

Vitreous Hemorrhage

- Characterised by diffuse T1-weighted hyperintense which does not drop in signal in fat saturated sequence and T2-weighted hypointense signal in vitreous humour.

Figure 6 (left) and (right) Axial T1-weighted MRI images of a 13-month-old boy with retinoblastoma of left eye. There is a T1-weighted hyperintense layer (arrow) in the dependent region of vitreous humour of left eye, with diffuse increase in T1-weighted hyperintense signal in rest of its vitreous humour (curved arrow) when comparing with contralateral eye. Features are suggestive of vitreous hemorrhage.

Aseptic orbital cellulitis and lens dislocation

- Retinoblastoma can promote inflammation of the globe leading to aseptic orbital cellulitis
- Under MRI, this is characterized by periocular T2-weighted hyperintense signal with contrast enhancement.
- Lens subluxation is seen often at the same time secondary to ciliary body necrosis.

Figure 7 (left) Oblique sagittal T1-weighted post contrast MRI image and (right) axial T2-weighted MRI image of a 13-month-old boy with left eye retinoblastoma. There is increase enhancement in periorbital soft tissue in left eye involving posterior to the orbital septum (arrow), suggestive of orbital cellulitis. There is also posterior subluxation of left lens shown in the T2-weighted image (arrow).

Post-laminar optic nerve invasion

- Presence of optic nerve invasion posterior to lamina cribrosa is a contraindication to intra-arterial chemotherapy and the segmented involved should be included for the enucleation to archive disease-free margin.
- Under MRI, the caliber of the involved optic nerve can be normal, while there can be abnormal enhancement or signal in the post-laminar segment to suggest involvement.

Figure 8 (left) Oblique sagittal T1-weighted post contrast MRI image (right) Axial T2-weighted MRI image of a 14-month-old boy with right eye retinoblastoma. There is subtle increase in contrast enhancement (arrow) and T2-weighted hyperintense signal (curved arrow) in the post-laminar segment of right optic nerve, suggestive of involvement by tumour.

Distant and systemic metastases

- The common sites include the lungs, liver, and marrow.
- Whole body imaging, including CT, MRI, scintigraphy or PET are helpful in evaluation the metastases.

R

Figure 9 (left) Coronal right knee radiograph and (right) coronal T2-weighted MRI image of a 10-year-old boy with surgical enucleation done bilateral retinoblastoma when he was 2 years old. The radiograph shows an ill-defined sclerotic lesion in medial metaphyseal region of proximal right tibia (arrow). MRI shows the lesion in the metaphyseal region of proximal tibia with extension into the epiphysis and cortical destruction (arrow). Biopsy was subsequently performed and confirmed retinoblastoma metastasis.

Conclusion

Retinoblastoma is the most common intra-ocular malignancy in children. Being familiar with the MRI features indicating advanced disease is important for pediatric radiologists for accurately staging the disease and guide the clinical team for subsequent management.

Reference

1. Fabian ID, Sagoo MS. Understanding retinoblastoma: epidemiology and genetics. Community Eye Health. 2018;31(101):7. PMID: 29915458; PMCID: PMC5998389.
2. Rauschecker AM, Patel CV, Yeom KW, Eisenhut CA, Gawande RS, O'Brien JM, Ebrahimi KB, Daldrup-Link HE. High-resolution MR imaging of the orbit in patients with retinoblastoma. Radiographics. 2012 Sep-Oct;32(5):1307-26. doi: 10.1148/rg.325115176. PMID: 22977020.
3. Ancona-Lezama D, Dalvin LA, Shields CL. Modern treatment of retinoblastoma: A 2020 review. Indian J Ophthalmol. 2020 Nov;68(11):2356-2365. doi: 10.4103/ijo.IJO_721_20. PMID: 33120616; PMCID: PMC7774148.
4. TNM8: The updated TNM classification for retinoblastoma. Community Eye Health. 2018;31(101):34. PMID: 29915471; PMCID: PMC5998398.
5. Fabian ID, Reddy A, Sagoo MS. Classification and staging of retinoblastoma. Community Eye Health. 2018;31(101):11-13. PMID: 29915461; PMCID: PMC5998397.

Comparison of Abdominal Ultrasonography and Radiography for Predicting Surgical Intervention in Necrotizing Enterocolitis: A Meta-analysis

A Difadyaputra[1], RC Putri[2]

[1] *Faculty of Medicine, Pembangunan Nasional "Veteran" Jakarta University, Indonesia*
[2] *Faculty of Medicine, Udayana University, Indonesia*

AOSPR 2024

Comparison of Abdominal Ultrasonography and Radiography for Predicting Surgical Intervention in Necrotizing Enterocolitis: A Meta-analysis

A. Difadyaputra [1] R.C.Putri [2]

Faculty of Medicine, Pembangunan Nasional "Veteran" Jakarta University . Faculty of Medicine, Udayana University

Background

Necrotizing enterocolitis (NEC) is a severe digestive condition that mostly impacts premature infants, leading to significant morbidity and mortality. Abdominal ultrasonography (AUS) is being used more frequently in combination with traditional abdominal radiography (AXR) to identify NEC and predicts its outcomes. However, there is a lack of studies evaluating the findings on both modalities to predict the need for surgery or mortality outcomes in NEC.

Purpose

To compare the findings of AUS and AXR in predicting the need for surgical intervention or mortality in NEC patients.

Methods

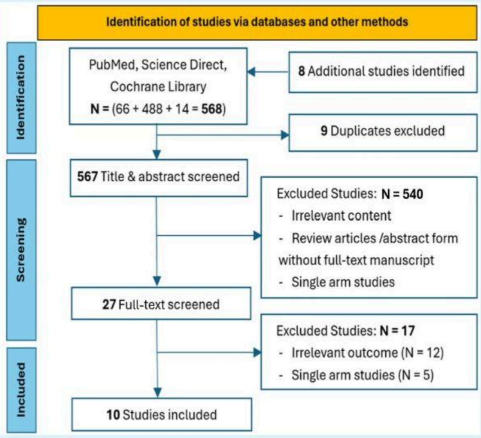

Inclusion Criteria

- Studies comparing AUS and AXR findings and and their association with surgical management or mortality outcomes in NEC.

Exclusion Criteria

- Abstract form without full-text manuscript, single-arm studies, case reports, review articles, languages other than English.
- Article/data cannot be accessed or extracted

Keywords

"(Necrotizing enterocolitis) AND (Ultrasonography OR sonography OR ultrasound) AND (abdominal x-ray OR abdominal radiograph OR abdominal radiography OR x-ray OR KUB)"

Outcomes

Surgery or death

Database

PubMed, Science Direct, and Cochrane Library

Results and Discussion

Study	Selection	Comparability	Outcome	Total Score	Quality
Muchantef et al, 2013	****	*	***	8	Good
Garbi-Goutel et al, 2013	****	*	***	8	Good
Staryszak et.al, 2015	***-	-	***	6	Fair
Prithviraj et. Al, 2015	****	-	***	7	Good
He et al, 2016	****	-	***	7	Good
Wang et al, 2016	****	*	***	8	Good
Lazow et al, 2021	****	*	***	8	Good
Chen et al, 2018	****	-	***	7	Good
Saad et al, 2018	****	*	***	8	Good
Yu et al, 2022	****	*	***	8	Good

Radiography findings	Studies (N)	Patients (N)	Odds Ratio	95% CI	p-value
Pneumatosis Intestinalis	9	381	2.34	1.23 – 4.46	0.009*
Pneumoperitoneum	8	58	13.35	4.15 – 42.92	<0.0001*
Portal Venous Gas	8	76	5.14	2.66 – 9.94	<0.00001*
Gasless Abdomen	3	101	1.07	0.42 – 2.71	0.89
Dilated Bowel	7	279	1.79	0.93 – 3.44	0.08
Bowel Wall Thickening	3	150	1.39	0.24 – 8.09	0.71

*A correlation was considered significant if $p<0.05$, N = Number

Ultrasonography findings	Studies (N)	Patients (N)	Odds Ratio	95% CI	p-value
Pneumatosis Intestinalis	10	262	2.36	1.45 – 3.83	0.0005*
Pneumoperitoneum	6	63	10.09	2.38 – 42.83	0.002*
Portal Venous Gas	8	140	2.29	1.08 – 4.87	0.03*
Echogenicity	3	56	2.61	1.17 – 5.80	0.02*
Bowel Wall Thickening	10	309	4.29	3.11 – 5.92	<0.00001*
Bowel Wall Thinning	7	63	3.91	1.30 – 11.76	0.02*
Absent/reduced peristaltic	7	257	7.37	2.99 – 18.16	<0.0001*
Focal Fluid Collection	7	108	5.88	1.96 – 17.66	0.002*
Simple Ascites	5	133	1.44	0.24 – 8.69	0.69
Complex Ascites	3	44	12.10	4.69 – 31.25	<0.00001*
Dilated Bowel	4	84	5.14	0.88 – 29.90	0.07
Increased Perfusion	4	82	4.75	1.24 – 18.17	0.02*

*A correlation was considered significant if $p<0.05$, N = Number

Imaging Modalities	Findings	Medical / No surgical group		Surgical or Death Group		OR	p-value
		Patients (T=688)	%	Patients (T=285)	%		
AUS	Pneumatosis	156	22.6	106	37.2	2.36	0.0005*
	Pneumoperitoneum	83	12	50	17.5	10.09	0.002*
	Portal venous gas	129	18.75	61	21.4	2.29	0.03*
	Bowel Wall Thickening	149	21.6	160	56.1	4.29	<0.00001*
	Dilated Bowel	32	4.6	52	18.2	5.14	0.07
AXR	Pneumatosis	260	37.8	121	42.4	2.34	0.009*
	Pneumoperitoneum	6	0.87	52	18.2	13.35	<0.0001*
	Portal venous gas	32	4.65	44	15.4	5.14	<0.00001*
	Bowel Wall Thickening	104	15.1	46	16.1	1.39	0.71
	Dilated Bowel	170	24.7	109	45.2	1.79	0.08

*A correlation was considered significant if $p<0.05$, T = Total

Among the 973 infants studied, 285 (29.3%) required surgery or died. The review included seven retrospective cohort studies, two prospective cohort studies, and one case series. Gestational ages ranged from 20 to 40 weeks, with birth weights from 540 to 4410 grams. NEC was diagnosed or symptoms appeared between 2 and 60 days of age.

Strength: First meta-analysis conducted to compare imaging modalities to predict surgical intervention or death in NEC.

Limitations: Small sample size, publication bias, variability in the studies

Conclusion

Pneumoperitoneum and complex ascites on AUS were strongly associated with the need for surgery or death, whereas only pneumoperitoneum on AXR had a strong association. Most AUS findings, apart from simple ascites and bowel dilation, correlate with the need for surgery or mortality in NEC. AUS offers additional insights that AXR cannot, including detailed visualization of abdominal wall, fluid, perfusion, peristalsis, and echogenicity. Future research should explore the advantages of combining both AXR and AUS for better predicting NEC outcomes.

Reference

1. Patel RM, Kandefer S, Walsh MC, Bell EF, Carlo WA, Laptook AR, et al. Causes and Timing of Death in Extremely Premature Infants from 2000 through 2011. New England Journal of Medicine. 2015 Jan 22;372(4):331–40.
2. Zani A, Pierro A. Necrotizing enterocolitis: controversies and challenges. F1000Research. 2015 Nov 30;4:1373.
3. Kim WY, Kim WS, Kim IO, Kwon TH, Chang W, Lee EK. Sonographic evaluation of neonates with early-stage necrotizing enterocolitis. Pediatric Radiology. 2005 Aug 3;35(11):1056–61.
4. Muchantef K, Epelman M, Darge K, Kirpalani H, Laje P, Anupindi SA. Sonographic and radiographic imaging features of the neonate with necrotizing enterocolitis: correlating findings with outcomes. Pediatric Radiology. 2013 Jun 15;43(11):1444–52.
5. Garbi-Goutel A, Brévaut-Malaty V, Panuel M, Michel F, Merrot T, Gire C. Prognostic value of abdominal sonography in necrotizing enterocolitis of premature infants born before 33 weeks gestational age. Journal of Pediatric Surgery. 2014 Apr;49(4):508–13.
6. He Y, Zhong Y, Yu J, Cheng C, Wang Z, Li L. Ultrasonography and radiography findings predicted the need for surgery in patients with necrotising enterocolitis without pneumoperitoneum. Acta Paediatrica. 2016 Jan 20;105(4).
7. Yu L, Liu C, Cui Y, Xue L, Ma L. Imaging manifestations of neonatal necrotizing enterocolitis to predict timing of surgery. The Turkish Journal of Pediatrics. 2022;64(4):632.
8. Prithviraj D, Sandeep B, Suresh A, Balaraju V, Mondal S. Comparison between x-ray and abdominal ultrasound findings of necrotizing enterocolitis, its usefulness in early diagnosis, prognosis, and to assess, is this is the time to change our view of surgeon's intervention according to the Bell's criteria. International Journal of Scientific Study. 2015 July;3(4):119–30.
9. Saad YG, Seif M, Mansi YA, Hashem RH. Role of Abdominal Ultrasonography in the assessment of Neonatal Necrotising Enterocolitis. The Egyptian Journal of Radiology and Nuclear Medicine. 2018 Sep 1;49(3):755–63.
10. Lazow SP, Tracy SA, Staffa SJ, Estroff JA, Parad RB, Castro-Aragon IM, et al. Abdominal ultrasound findings contribute to a multivariable predictive risk score for surgical necrotizing enterocolitis: A pilot study. American Journal of Surgery. 2021 Nov;222(5):1034–9.

A Comparison of Automatic Bone Age Assessments between the Left and Right Hands: A Tool for Filtering Measurement Errors

Saelin Oh[1], Yeo Eun Han[1], Kyu-Chong Lee[1], Jae-Joon Lee[2], Chang Ho Kang[1], Kyung-Sik Ahn[1]

[1] Department of Radiology, Anam Hospital, Korea University College of Medicine, Republic of Korea
[2] Crescom, Seongnam, Republic of Korea

A Comparison of Automatic Bone Age Assessments between the Left and Right Hands: A Tool for Filtering Measurement Errors

Saelin Oh[1], Yeo Eun Han[1], Kyu-Chong Lee[1], Jae-Joon Lee[2], Chang Ho Kang[1] and Kyung-Sik Ahn[1]

[1] Department of Radiology, Anam Hospital, Korea University College of Medicine
[2] Crescom, Seongnam, Republic of Korea

Background

- Bone age assessment (BAA) is a clinical procedure used to evaluate skeletal maturity in pediatric patients .
- Various automatic and deep learning methods for BAA have been proposed, which have demonstrated high accuracy, reproducibility, and time efficiency.
- It is time to focus on how to use it efficiently in real practice without missing inevitable errors.

Purpose

- To introduce an upgraded automatic hand bone alignment technique and to propose right-hand BAA as a tool for filtering out measurement errors

Materials and Methods

- Our study included 757 children underwent bilateral radiography at our institution between January and December 2023.
- The digital images were processed using an automated MediAI-BA method; the model relies on hybrid TW3 and GP AI-based automatic bone age measurements.
- The absolute difference between each hand BAA by the model (ADBH model) was calculated. Bland–Altman, Passing–Bablok, and Spearman correlation coefficients were analyzed.

Results

Variables	ADBH Model ≤ 0.5 Year (n = 698)	ADBH Model > 0.5 Year (n = 59)	P
Age, years	8.77 ± 2.66	8.55 ± 2.73	0.555
Male-to-female ratio	295:403	26:33	0.788
Left-hand BAA	9.18 ± 3.21	8.78 ± 2.27	0.356
Right-hand BAA	9.22 ± 3.22	9.00 ± 3.39	0.620
ADBH model	0.198 ± 0.145 (0.187, 0.209)	0.667 ± 0.109 (0.638, 0.695)	<0.001
Developmental stage			0.025
Pre-puberty	201/698 (28.2%)	26/59 (44.1%)	0.018
Early and mid-puberty	462/698 (66.2%)	29/59 (49.2%)	0.010
Late puberty	28/698 (4.0%)	2/59 (3.4%)	1.000
Post puberty	7/698 (1.0%)	2/59 (3.4%)	0.151

Table1. A comparison of the characteristics of the study population

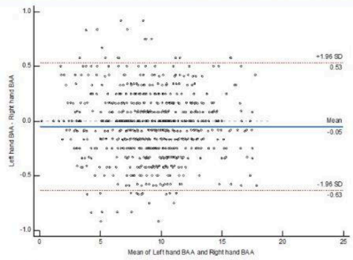

Figure1. The Bland–Altman plots indicate an agreement between each hand's bone age assessment. The dotted horizontal lines represent a standard deviation of ± 2.

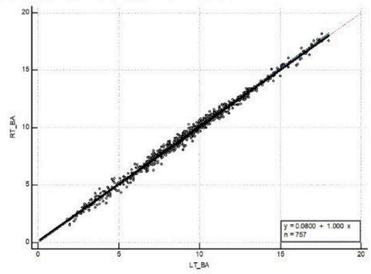

Figure2. The Passing–Bablok regression analysis showed that the overall correlation of the bone age assessment between both hands was excellent, with no significant deviation from linearity in this association (p = 0.15).

	Left Hand	Right Hand	P
Automatic bone age assessment by the model	8.78 ± 3.27	9.00 ± 3.39	0.011
Reference standard bone age reference by two reviewers	8.93 ± 3.29	8.89 ± 3.33	0.157
Mean absolute difference	0.409 ± 0.335 (0.322, 0.467)	0.424 ± 0.329 (0.339, 0.510)	0.809
Median	0.354	0.330	
Range	0–1.75	0–1.33	

Tabe2. A comparison of the bone age assessment by the model and the reference standard.

Conclusions

- Our study showed an excellent overall correlation of BAAs between both hands using the model and provided the possibility of using the right-hand BAA as a validation tool.
- Perceptible differences between each hand may indicate a large measurement error and thus may be a signal for manual supervision.

TOP 5 ORAL PRESENTATIONS

Clinical Prognostication in Acute Necrotizing Encephalopathy of Childhood: Role of MR Imaging Severity Assessment

Kiran Hilal

Department of Radiology, Aga Khan University Hospital, Karachi, Pakistan

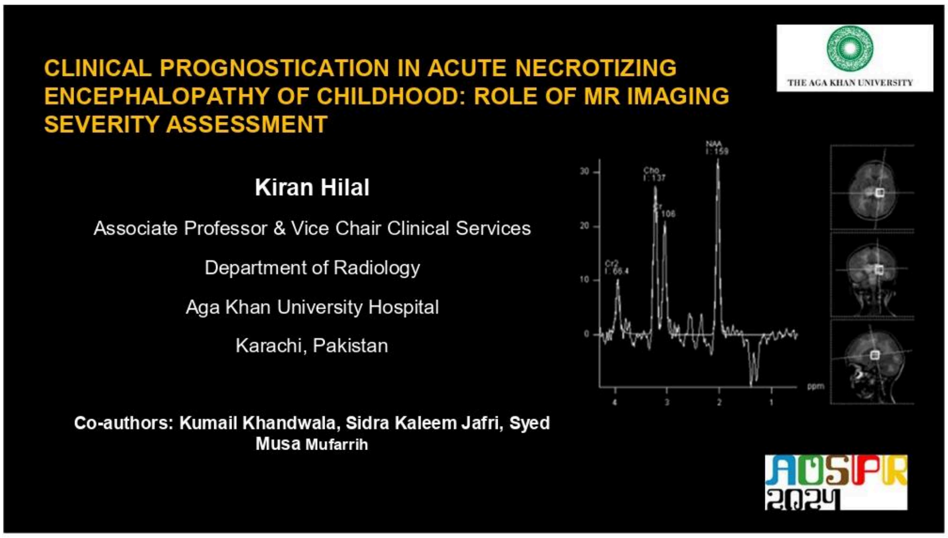

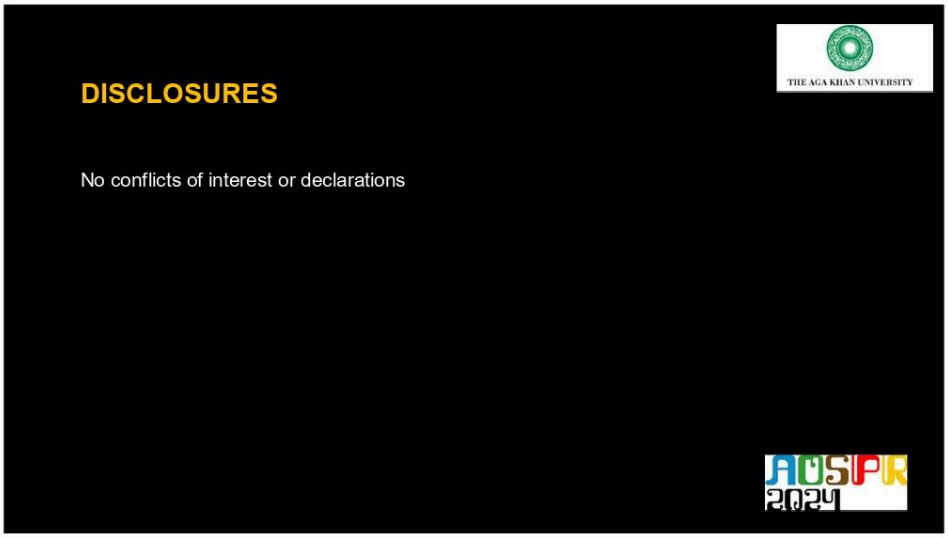

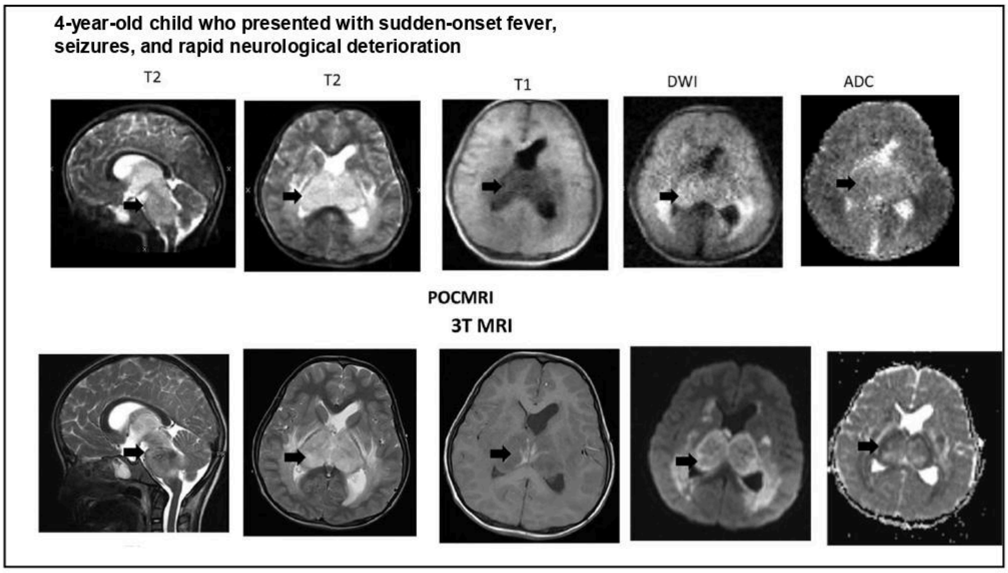
4-year-old child who presented with sudden-onset fever, seizures, and rapid neurological deterioration
T2
T2
T1
DWI
ADC
POCMRI
3T MRI

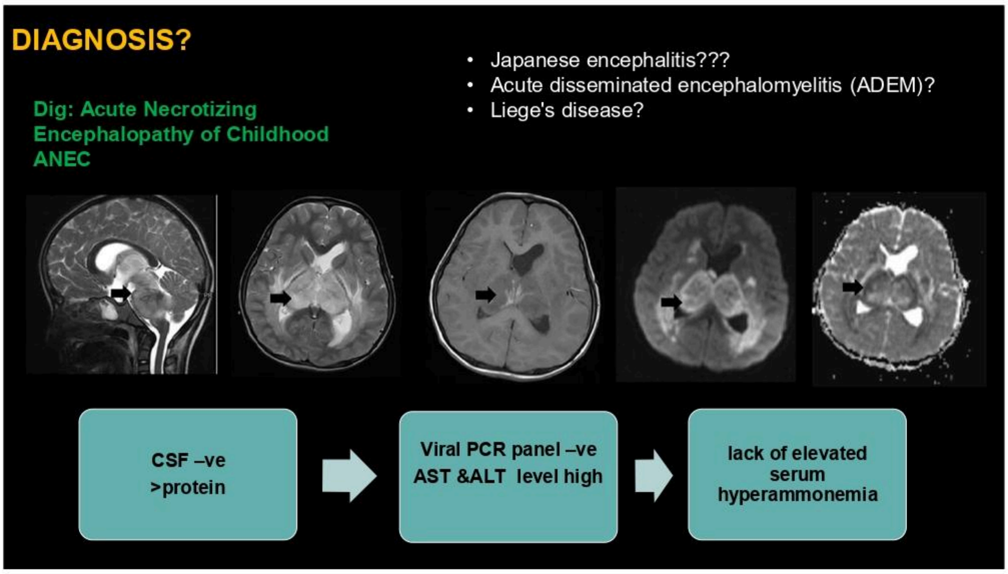
DIAGNOSIS?
Dig: Acute Necrotizing Encephalopathy of Childhood ANEC
Japanese encephalitis???
Acute disseminated encephalomyelitis (ADEM)?
Liege's disease?
CSF –ve
>protein
Viral PCR panel –ve
AST &ALT level high
lack of elevated serum hyperammonemia

BACKGROUND

- Acute Necrotizing Encephalopathy (ANEC) is a rare, rapidly progressive, and often fatal condition that predominantly affects children, usually following viral infections. It primarily targets the thalami, brainstem, and cerebellum, leading to devastating neurological outcomes.
- It is primarily reported in Asian countries like Japan, Taiwan, Korea, and the subcontinent and has a variable prognosis till date.

CURRENT CHALLENGE

- The current imaging criteria for diagnosing and predicting clinical outcomes in ANEC face significant challenge

Study	Key Features	Limitations
Wong et al. (2006)	Correlation between MRI (thalamic lesions) and clinical outcomes.	Small sample size, no comprehensive score. But the problem with this limitation was
Yamamoto et al. (2015)	Developed a severity score based on lesion location and extent.	Complex to apply, limited validation.
Wu et al. (2015)	Clinicoradiologic approach, highlighted underdiagnosis.	No formal scoring system.

1. **Current MR imaging criteria are too complex and variable.**
2. **Heterogeneity in MR scoring systems.**
3. **Validation on small cohorts.**

A SIMPLIFIED IMAGING APPROACH

- **Rationale & Need for Study:**
- **There is a lack of a standardized tool for predicting ANEC. prognosis**

- A **simplified MR-based score** can improve diagnostic accuracy.

- This study leverages the **largest cohort from South Asia**, addressing a crucial gap in current knowledge

THE AGA KHAN UNIVERSITY

AOSPR 2024

THE AGA KHAN UNIVERSITY

A SIMPLIFIED IMAGING APPROACH

- **Objective:**
- **Develop a simplified , more robust and widely applicable and practical MR scoring system to improve the diagnosis and clinical prognostication of ANEC**

AOSPR 2024

MATERIALS & METHODS

- Retrospective cross-sectional study.
- Study period: 13 years (from 2010 to 2023)
- Inclusion criteria: pediatric patients with ANEC meeting Mizuguchi's criteria.
- Other diseases resembling ANEC were excluded from the study.

Mizuguchi's criteria

- Acute encephalopathy (defined as a sudden decline in consciousness and/or behavioral changes like confusion or irritability)
- The lack of elevated serum hyperammonemia
  >ALT levels
- The absence of cerebrospinal fluid (CSF) pleocytosis but raised proteins
- Characteristic neuroimaging features displaying bilateral lesions in the thalami

9

Mizuguchi M, Abe J, Mikkaichi K, Noma S, Yoshida K, Yamanaka T, Kamoshita S (1995) Acute necrotizing encephalopathy of childhood: a new syndrome presenting with multifocal, symmetric brain lesions. J Neurol Neurosurg Psychiatry 58:555–561

IMAGING ASSESSMENT

- MR Imaging Examination and Score Development:
- Two pediatric radiologists independently assessed MR imaging variables.
- Developed a simplified MR-based imaging score for acute necrotizing encephalopathy by integrating and modifying approaches from Wong et al. and Ibrahim et al.

- *Wong AM, Simon EM, Zimmerman RA, Wang HS, Toh CH, Ng SH (2006) Acute necrotizing encephalopathy of childhood: Correlation of MR findings and clinical outcome. AJNR Am J Neuroradiol 27:1919-1923.*
- *Ibrahim RSM, Elzayat W, Seif HM, El-Kiki HA, Emad-Eldin S, Shahin M, Kamel SM, Osama R, Zakaryia R, Fatouh M, Hachem RH (2020) Multi-parametric magnetic resonance imaging in acute necrotizing encephalopathy of children: validity and prognostic value. Egypt J Radiol Nucl Med 51:113.*

IMAGING SCORE

1. **Imaging Severity Markers:**
    1. Hemorrhage
    2. Cavitation
    3. Enhancement,
    4. Diffusion Restriction
2. **Involvement of key anatomical regions:**

    5.Basal ganglia

    6.Cerebellum

    7.Brainstem

    8.Cerebral white matter

We initially associated these parameters with clinical outcomes and found that diffusion restriction and cerebellar involvement were the most significant.

- These were given 2 points each, while other parameters were given 1 each.
- The total score, ranging from 0 to 10, was categorized into mild (0-3), moderate (4-7), and severe (8-10).

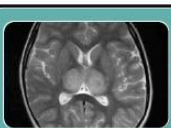

Cavitation
Cavitation was defined as those lesions having sharply defined margins, and CSF intensity with hypointense signal on T1-weighted images and hyperintensity on T2-weighted images with rim enhancement on post contrast images.

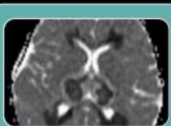

Diffusion restriction
Diffusion restriction was defined by cytotoxic edema appearing bright on diffusion weighted sequences (DWI) and showing dropout on corresponding apparent diffusion coefficient (ADC) maps.

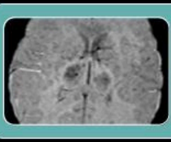

Hemorrhage
The presence of hemorrhage was defined as either petechial or macro-hemorrhages showing signal dropout on SWI sequences.

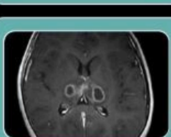

Enhancement
Enhancement was considered positive and defined as either rim enhancement, heterogeneous or intense/avid on T1-post contrast images.

CLINICAL OUTCOME

Clinical outcomes were determined at the time of discharge and on follow-ups by a pediatric neurologist using modified Rankin Scale with scores 0 to 6 ranging from:

- No/mild disability (0 to 2)
- Moderate disability (3 to 4)
- Severe disability (4 to 6)
- Death

13

STATISTICAL ANALYSIS

- SPSS version 20.0.
- Chi-square test, ¥ Fisher Exact Test, € One way ANOVA test was used for statistical analysis and to measure associations.
- P-values less than 0.05 were considered statistically significant.
- **Cohen's Kappa (k)Strength of agreement**

14

THE AGA KHAN UNIVERSITY

RESULTS

CORRELATION WITH CLINICAL PARAMETERS

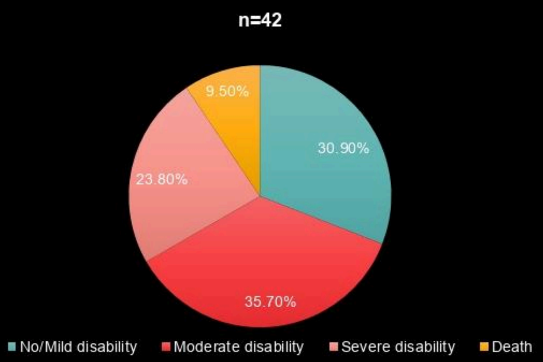

- The clinical outcomes were not significantly associated with
  - length of stay
  - platelet count
  - serum alanine aminotransferase level.
- Presence of shock had a statistically significant association with a worse clinical outcome (p-0.01).
- .

15

AOSPR 2024

RESULTS

Table 2: MR findings and associations with clinical outcome in patients with acute necrotizing encephalopathy of childhood.

	No/Mild Disability (n=13)	Moderate Disability (n=15)	Severe Disability (n=10)	Death (n=4)	P-value
Basal Ganglia	07 (53.8%)	09 (60%)	04 (40%)	03 (75%)	0.6¥
Cerebral White Matter	09 (69.2%)	08 (53.3%)	09 (90%)	03 (75%)	0.2ǂ
Cerebellum	07 (53.8%)	03 (20%)	03 (30%)	03 (75%)	0.05*¥
Brainstem	10 (77%)	09 (60%)	07 (70%)	04 (100%)	0.5ǂ
Mamillary Bodies	01 (7.7%)	01 (6.7%)	0 (0.0%)	01 (25%)	0.5ǂ
External Capsule	03 (23.1%)	05 (33.3%)	04 (40%)	02 (50%)	0.6ǂ
Hemorrhage	06 (46.2%)	07 (46.7%)	04 (40%)	03 (75%)	0.7¥
Cavitation	05 (38.5%)	05 (33.3%)	05 (50%)	03 (75%)	0.4¥
Enhancement	06 (46.1%)	07 (46.7%)	02 (20%)	03 (75%)	0.2¥
Diffusion Restriction	07 (53.8%)	12 (80%)	09 (90%)	04 (100%)	0.03*ǂ

* P-value <0.05, ¥ Chi-square test, ǂ Fisher Exact Test

RESULTS

MR Imaging Score Grading	Clinical Outcome			
	Mild disability	Moderate disability	Worst Outcome	P-value
Mild (0 to 3)	8 (44.4)	7 (38.9)	3 (16.7)	0.027* ǂ
Moderate (4 to 7)	2 (10.5)	9 (47.4)	8 (42.1)	
Severe (8 to 10)	0 (0)	1 (20)	4 (80)	
Mean MR Imaging Scores	3 ± 2.21	4.35 ± 2.11	6.13 ± 2.38	0.004* †

* P-value <0.05 was considered as statistically significant

ǂ: Fischer exact test, † One Way ANOVA

RESULTS

Table 3: Inter-rater reliability for different predictors of MRI severity

MR Variables	Percent agreement	Expected agreement (%)	Cohen's Kappa (k)
Thalami	100	-	-
Basal ganglia	90.48	49.89	0.81
Cerebral white matter	78.57	51.36	0.55
Cerebellum	92.86	53.40	0.84
Brainstem	80.95	52.83	0.60
Hemorrhage	95.24	51.02	0.90
Diffusion restriction	90.48	55.1	0.78
Cavitation	78.57	64.97	0.38
Enhancement	76.19	54.54	0.47

Key

Cohen's Kappa (k)	Strength of agreement
0.8 ≥ k	Excellent agreement
0.4 ≤ k < 0.8	Mild to moderate agreement
K<0.4	Poor agreement

Excellent intra-observer reliability with scores of 96% and 93%, respectively

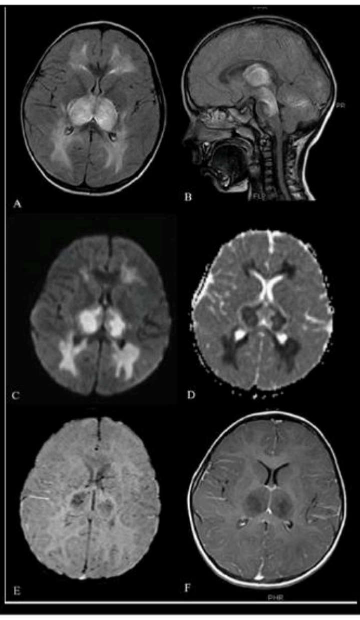

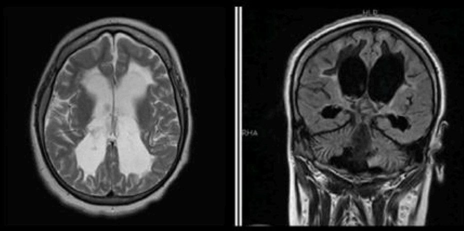

3 yrs old
MR imaging score of 8 with severe long-term disability

DISCUSSION

Key Findings

- A simplified MR-based scoring system was developed, integrating, imaging severity markers, and anatomical locations.
- Diffusion restriction and cerebellar involvement were the most predictive of bad clinical outcomes in ANEC.
- Reliable correlation between imaging findings and clinical prognosis was established, making this scoring system practical in real-world settings.

Kim JH, Kim IO, Lim MK, Park MS, Choi CG, Kim HW, Kim JE, Choi SJ, Koh YH, Yang DM, Choo SW, Chung MJ, Yoon HK, Goo HW, Lee M (2004) Acute necrotizing encephalopathy in Korean infants and children: imaging findings and diverse clinical outcome. Korean J Radiol 5:171-177.

DISCUSSION

Comparison to Previous Studies

Brainstem Involvement: Previous studies suggested favorable recovery with brainstem involvement, but in our study, all patients who died had brainstem involvement, though this was not statistically significant.

Hemorrhage and Cavitation: Contrary to Kim et al.'s findings, our study found no significant association between hemorrhage (47.6%) or cavitation (42.9%) and poorer clinical outcomes.

21

Kim JH, Kim IO, Lim MK, Park MS, Choi CG, Kim HW, Kim JE, Choi SJ, Koh YH, Yang DM, Choo SW, Chung MJ, Yoon HK, Goo HW, Lee M (2004) Acute necrotizing encephalopathy in Korean infants and children: imaging findings and diverse clinical outcome. Korean J Radiol 5:171-177.

DISCUSSION

Comparison to Previous Studies

Mortality Rate: Our study showed a mortality rate of 9.5%, significantly lower than the up to 65% reported in previous studies.

Novel Approach: Unlike previous studies, ours uniquely assessed the impact of individual imaging severity and anatomical parameters on clinical outcomes

22

Kim JH, Kim IO, Lim MK, Park MS, Choi CG, Kim HW, Kim JE, Choi SJ, Koh YH, Yang DM, Choo SW, Chung MJ, Yoon HK, Goo HW, Lee M (2004) Acute necrotizing encephalopathy in Korean infants and children: imaging findings and diverse clinical outcome. Korean J Radiol 5:171-177.

LIMITATIONS

- Single center study, relatively small sample size due to disease rarity
- We had no resources to carry out the RANBP2 target mutation and therefore could not determine a genetic analysis.
- Timing of MR brain scans was not considered, and some features may have been underrepresented since radiological features of ANEC (such as hemorrhage and cavitation) can evolve over time.
- Our follow-ups were limited because not all patients could be clinically examined, and we had few patients with follow-up imaging.

CONCLUSION & FUTURE DIRECTIONS

- ANEC's **complexity** demands a robust MR-based severity scoring system for better diagnosis and outcomes prediction
- Diffusion restriction and cerebellar involvement are crucial for prognostication
- **Future direction**: Standardized imaging protocols and genetic testing will help refine and validate the current scoring system for better patient outcomes

Wong AM, Simon EM, Zimmerman RA, Wang HS, Toh CH, Ng SH (2006) Acute necrotizing encephalopathy of childhood: Correlation of MR findings and clinical outcome. AJNR Am J Neuroradiol 27:1919-1923.


The Aga Khan University
THE AGA KHAN UNIVERSITY
Thank You
Questions?
Email: kiran.hilal@aku.edu
@KiranHilal1
linkedin.com/in/dr-kiran-hilal
Kiran Hilal
AOSPR 2024

A Pictorial Review of Paediatric Head and Neck Masses

Nadia Fareeda Muhammad Gowdh[1,2,3], Faizah Mohd Zaki[2], Rohazly Ismail[3]

[1] _Biomedical Imaging Department, Faculty of Medicine, Universiti Malaya, Malaysia_
[2] _Radiology Department, Children Specialist Hospital, Universiti Kebangsaan Malaysia, Malaysia_
[3] _Radiology Department, Hospital Tunku Azizah, Kuala Lumpur, Malaysia_

22nd Annual Scientific Meeting of Asian and Oceanic Society for Pediatric Radiology (AOSPR) 2024

1

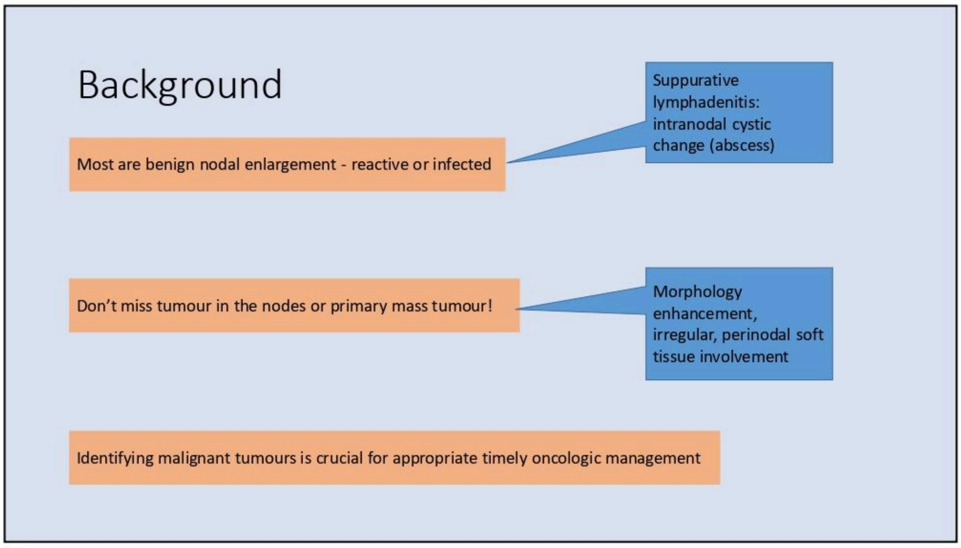

2

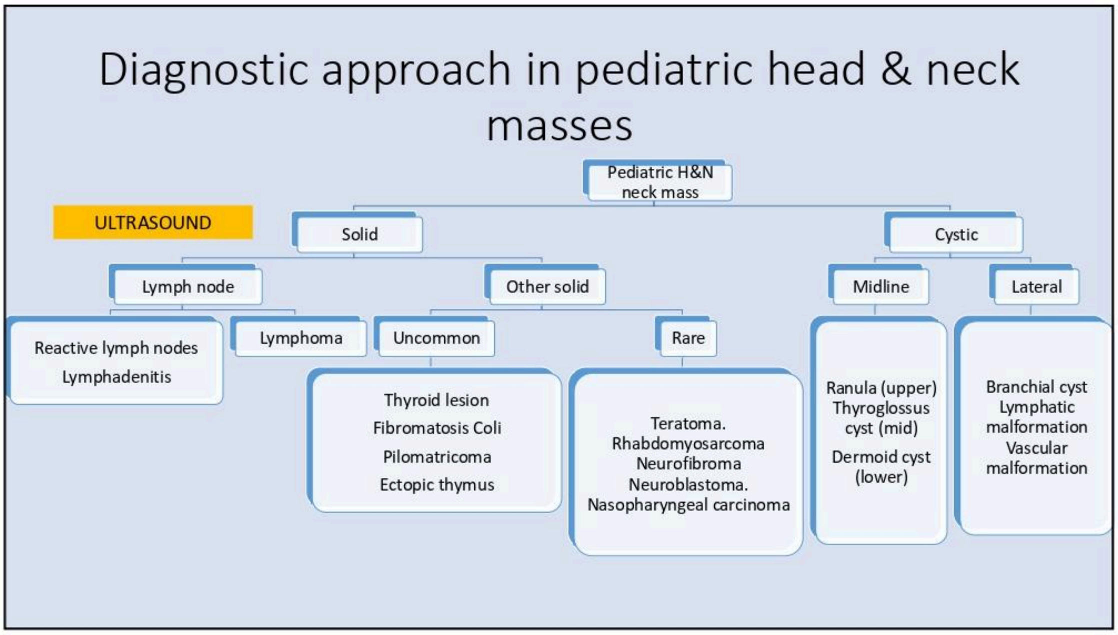
Diagnostic approach in pediatric head & neck masses
Pediatric H&N neck mass
ULTRASOUND
Solid
Cystic
Lymph node
Other solid
Midline
Lateral
Reactive lymph nodes
Lymphadenitis
Lymphoma
Uncommon
Rare
Thyroid lesion
Fibromatosis Coli
Pilomatricoma
Ectopic thymus
Teratoma.
Rhabdomyosarcoma
Neurofibroma
Neuroblastoma.
Nasopharyngeal carcinoma
Ranula (upper)
Thyroglossus cyst (mid)
Dermoid cyst (lower)
Branchial cyst
Lymphatic malformation
Vascular malformation

3

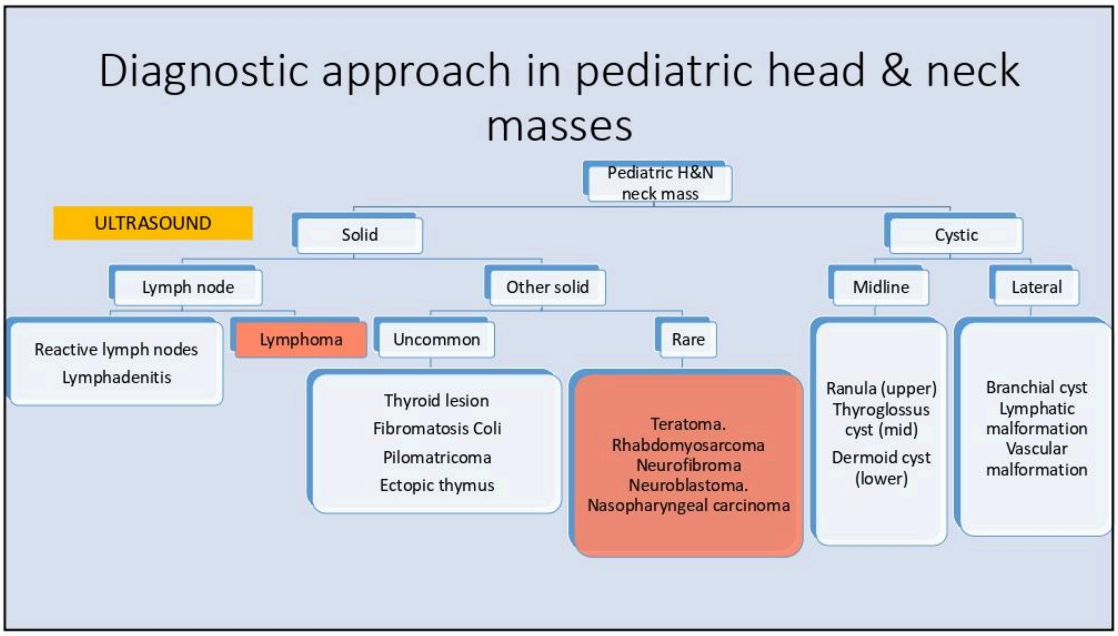
Diagnostic approach in pediatric head & neck masses
Pediatric H&N neck mass
ULTRASOUND
Solid
Cystic
Lymph node
Other solid
Midline
Lateral
Reactive lymph nodes
Lymphadenitis
Lymphoma
Uncommon
Rare
Thyroid lesion
Fibromatosis Coli
Pilomatricoma
Ectopic thymus
Teratoma.
Rhabdomyosarcoma
Neurofibroma
Neuroblastoma.
Nasopharyngeal carcinoma
Ranula (upper)
Thyroglossus cyst (mid)
Dermoid cyst (lower)
Branchial cyst
Lymphatic malformation
Vascular malformation

4

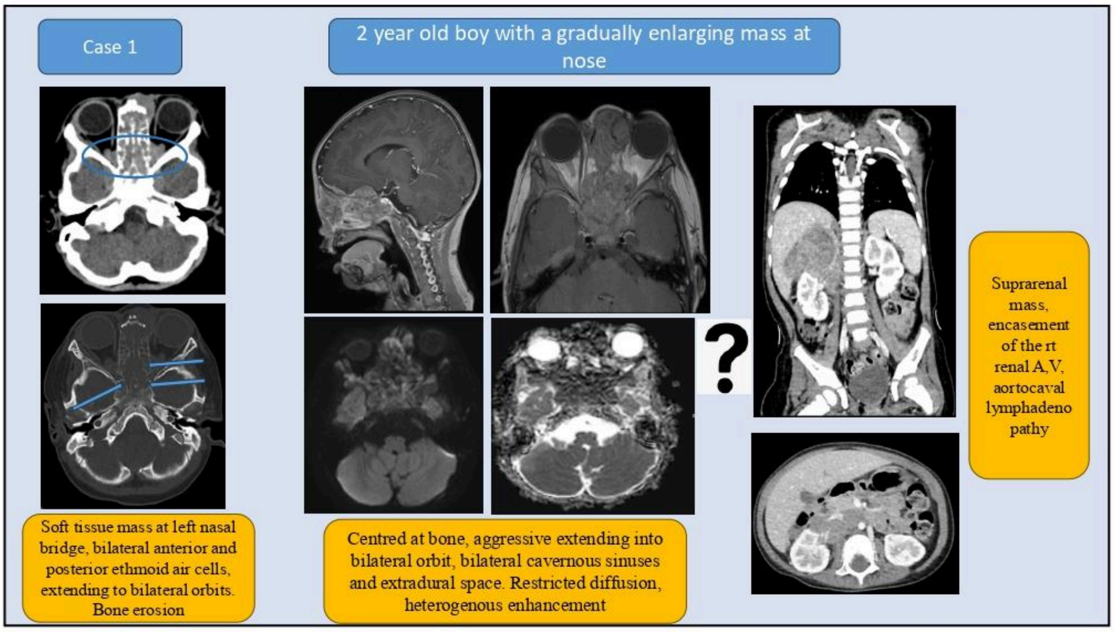
Case 1
2 year old boy with a gradually enlarging mass at nose
?
Suprarenal mass, encasement of the rt renal A,V, aortocaval lymphadeno pathy
Soft tissue mass at left nasal bridge, bilateral anterior and posterior ethmoid air cells, extending to bilateral orbits. Bone erosion
Centred at bone, aggressive extending into bilateral orbit, bilateral cavernous sinuses and extradural space. Restricted diffusion, heterogenous enhancement

5

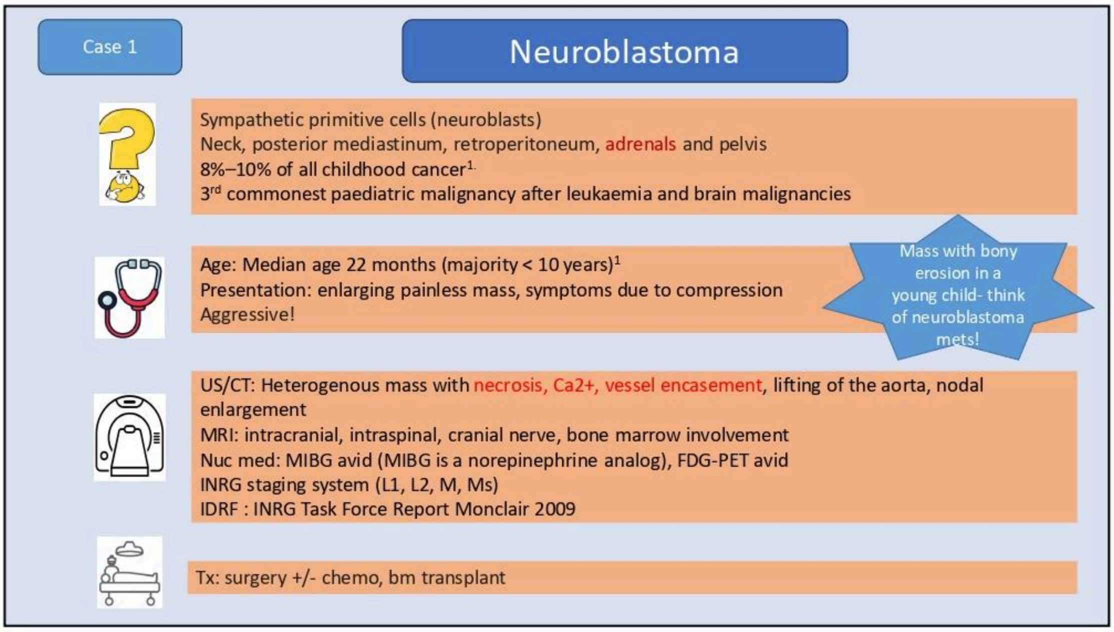
Case 1
Neuroblastoma
Sympathetic primitive cells (neuroblasts)
Neck, posterior mediastinum, retroperitoneum, adrenals and pelvis
8%–10% of all childhood cancer1.
3rd commonest paediatric malignancy after leukaemia and brain malignancies
Age: Median age 22 months (majority < 10 years)1
Presentation: enlarging painless mass, symptoms due to compression
Aggressive!
Mass with bony erosion in a young child- think of neuroblastoma mets!
US/CT: Heterogenous mass with necrosis, Ca2+, vessel encasement, lifting of the aorta, nodal enlargement
MRI: intracranial, intraspinal, cranial nerve, bone marrow involvement
Nuc med: MIBG avid (MIBG is a norepinephrine analog), FDG-PET avid
INRG staging system (L1, L2, M, Ms)
IDRF : INRG Task Force Report Monclair 2009
Tx: surgery +/- chemo, bm transplant

6

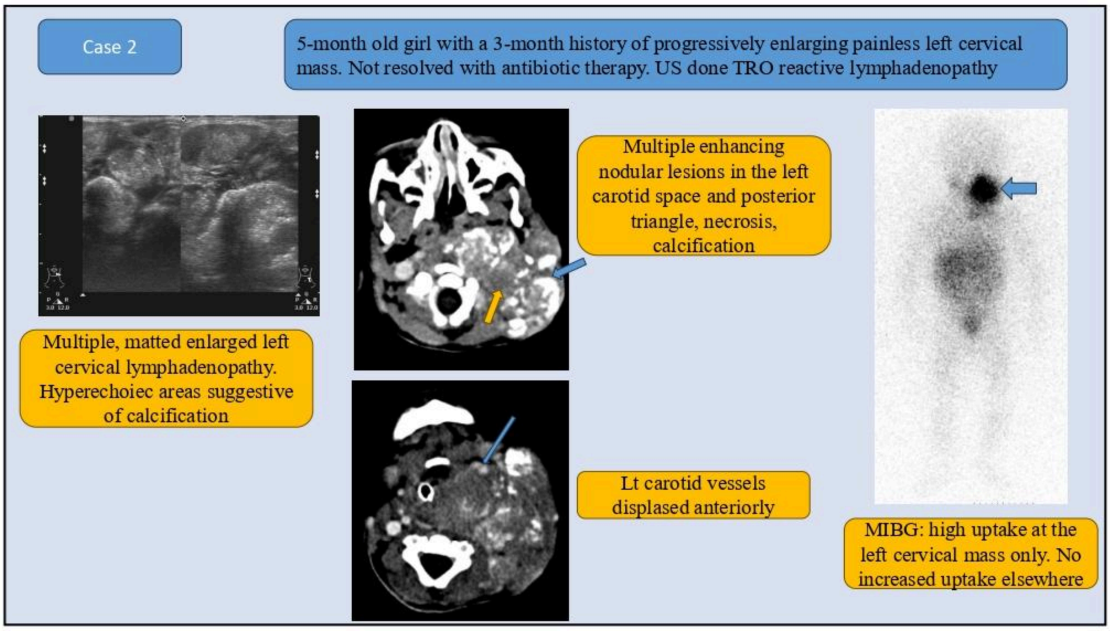

7

Case 2

Primary cervical neuroblastoma

Incidence of primary cervical neuroblastoma : < 5% of all neuroblastomas[2]
Arises from the superior cervical ganglion behind the ICA
Posterior to the vascular sheet, displacing the carotid artery, IJV anteriorly

Age: More common in infants[2]
Presentation: Enlarging painless lateral neck mass, symptoms due to compression
Ds pattern: Aggressive behavior - can invade the cranial nerves

Ultrasound usually primary imaging tool
CT/MRI for further characterization (MRI superior)

Tx: surgery
Favourable outcome of infant neuroblastoma.
The overall five-year survival rate of cervical neuroblastoma is around 90% [2]

8

Case 3

5 year old boy with left neck swelling x 2weeks. External CT noted to have left neck mass.


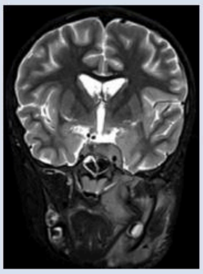
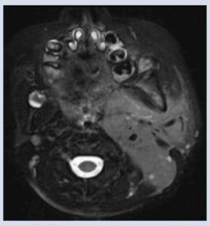
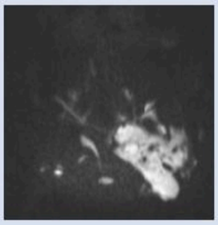
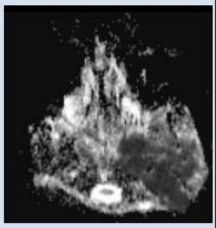

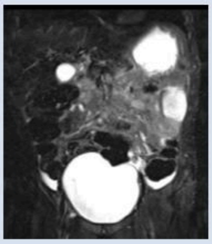

Matted enlarged left cervical lymphadenopathy, palatine tonsil, adenoid involvement with restricted diffusion, prominent right cervical node, bilateral cavernous sinus and rt renal, abdominal nodal involvement

9

Case 3

Burkitt lymphoma (Non-Hodgkin Lymphoma)

Aggressive B-cell lymphoma predominantly affecting children
Most common (40%) type of non-Hodgkin lymphoma in childhood

Age: Median age is 8 years[4]
Male predominance (M:F = 4:1)
Presentation: enlarging mass
Beware of airway compromise!

Ultrasound, CT/MRI
Solid lobulated mass, predilection for the Waldeyer's ring, restricted diffusion (highly cellular), T2W isointense (highly cellular), homogenous enhancement
(absence of necrosis and bone destruction supports Burkitt's lymphoma)[5]

Curable, highly sensitive to chemotherapy

10

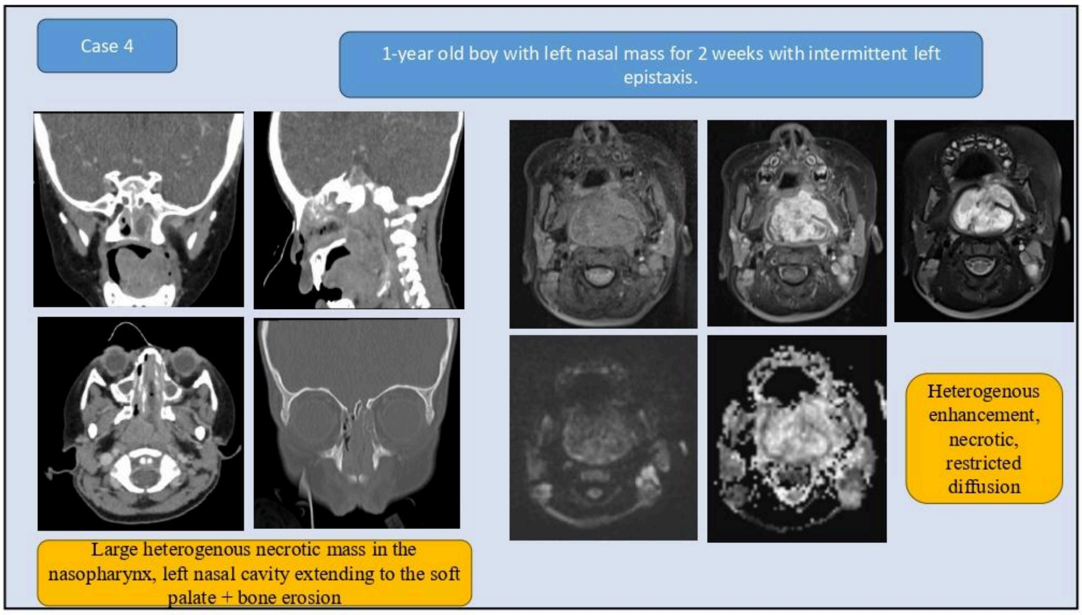
Case 4
1-year old boy with left nasal mass for 2 weeks with intermittent left epistaxis.
Heterogenous enhancement, necrotic, restricted diffusion
Large heterogenous necrotic mass in the nasopharynx, left nasal cavity extending to the soft palate + bone erosion

11

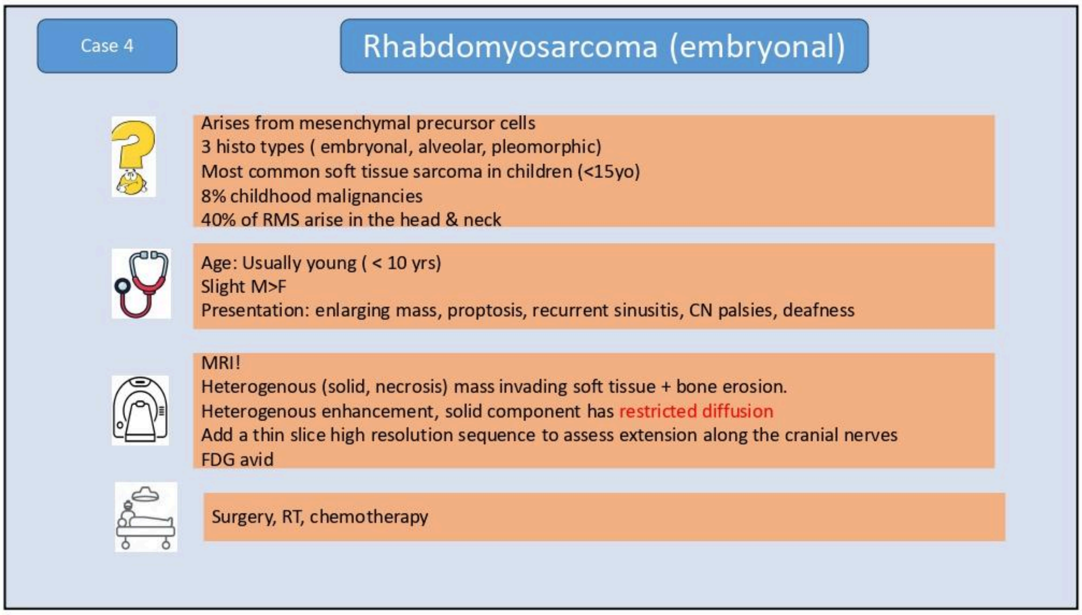
Case 4
Rhabdomyosarcoma (embryonal)
Arises from mesenchymal precursor cells
3 histo types (embryonal, alveolar, pleomorphic)
Most common soft tissue sarcoma in children (<15yo)
8% childhood malignancies
40% of RMS arise in the head & neck
Age: Usually young (< 10 yrs)
Slight M>F
Presentation: enlarging mass, proptosis, recurrent sinusitis, CN palsies, deafness
MRI!
Heterogenous (solid, necrosis) mass invading soft tissue + bone erosion.
Heterogenous enhancement, solid component has restricted diffusion
Add a thin slice high resolution sequence to assess extension along the cranial nerves
FDG avid
Surgery, RT, chemotherapy

12

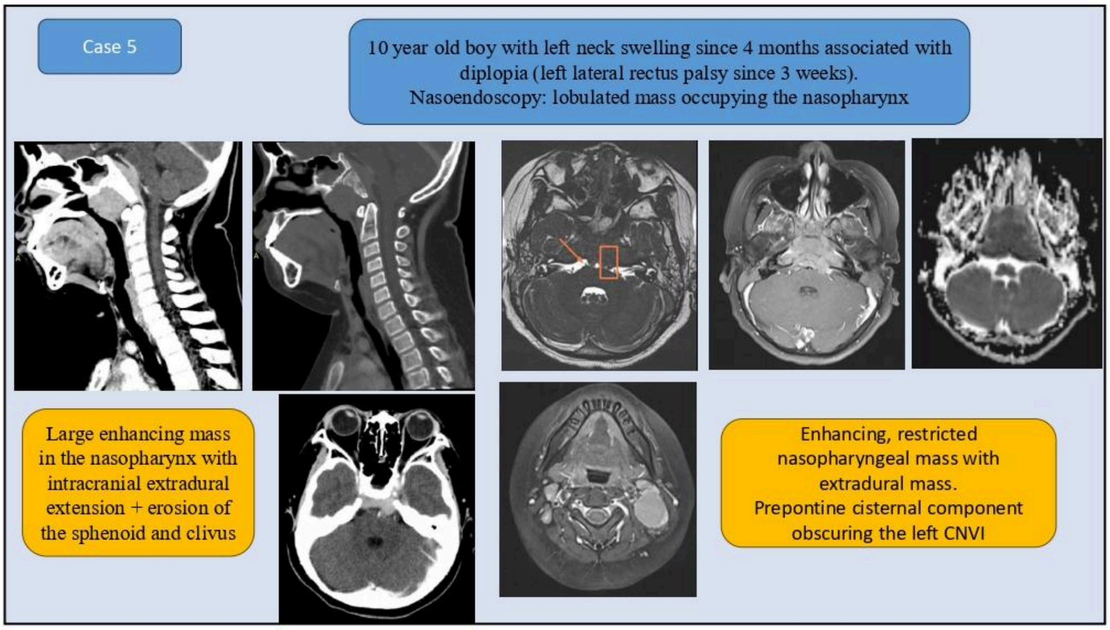
Case 5
10 year old boy with left neck swelling since 4 months associated with diplopia (left lateral rectus palsy since 3 weeks).
Nasoendoscopy: lobulated mass occupying the nasopharynx
Large enhancing mass in the nasopharynx with intracranial extradural extension + erosion of the sphenoid and clivus
Enhancing, restricted nasopharyngeal mass with extradural mass.
Prepontine cisternal component obscuring the left CNVI

13

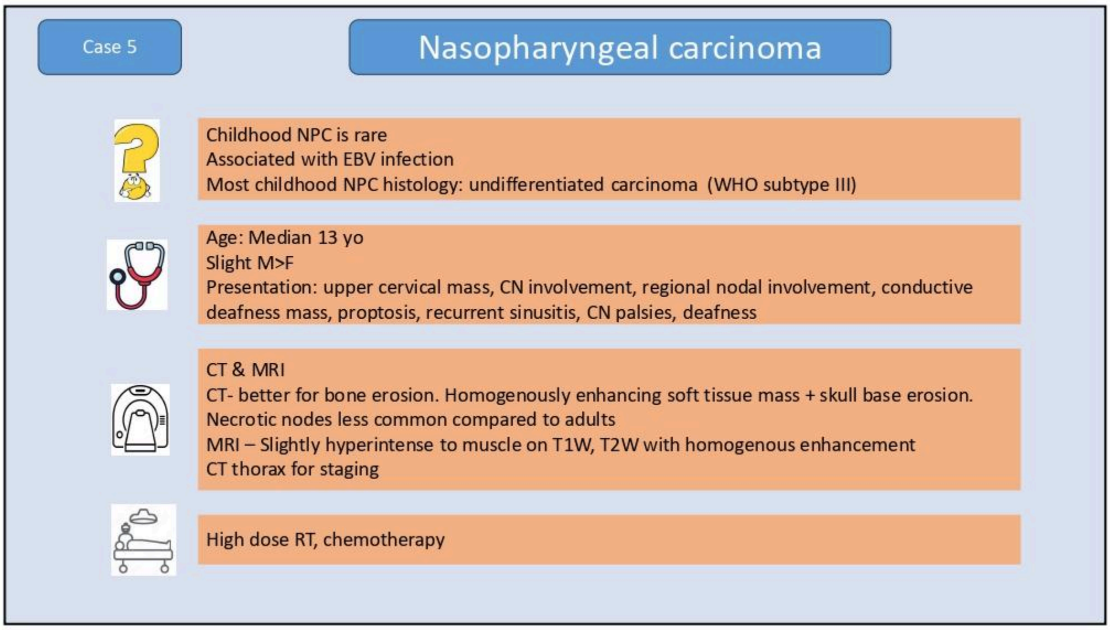
Case 5
Nasopharyngeal carcinoma
Childhood NPC is rare
Associated with EBV infection
Most childhood NPC histology: undifferentiated carcinoma (WHO subtype III)
Age: Median 13 yo
Slight M>F
Presentation: upper cervical mass, CN involvement, regional nodal involvement, conductive deafness mass, proptosis, recurrent sinusitis, CN palsies, deafness
CT & MRI
CT- better for bone erosion. Homogenously enhancing soft tissue mass + skull base erosion.
Necrotic nodes less common compared to adults
MRI – Slightly hyperintense to muscle on T1W, T2W with homogenous enhancement
CT thorax for staging
High dose RT, chemotherapy

14

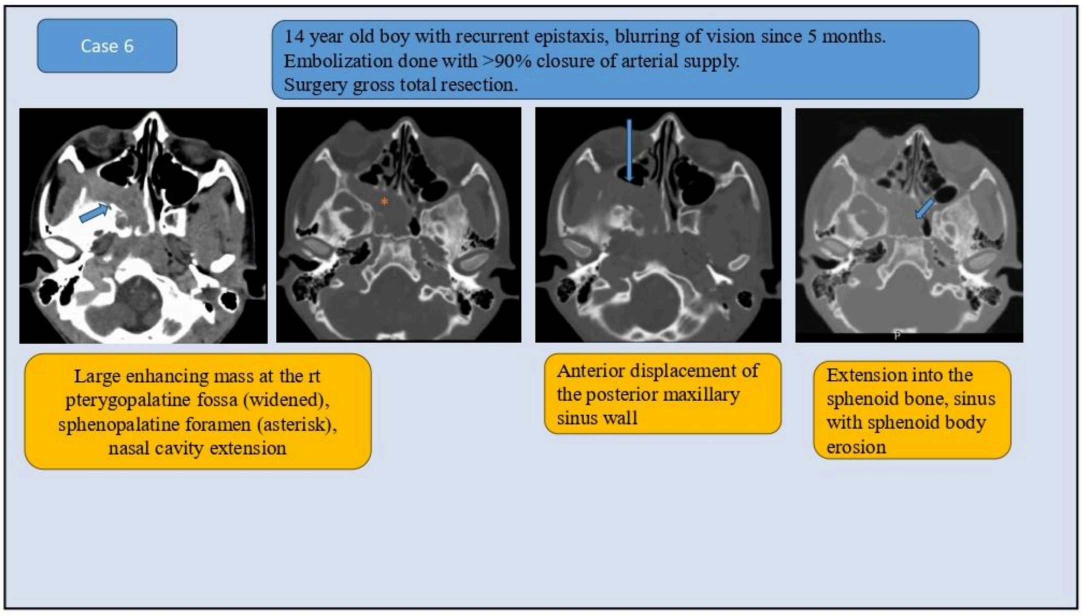
Case 6
14 year old boy with recurrent epistaxis, blurring of vision since 5 months.
Embolization done with >90% closure of arterial supply.
Surgery gross total resection.
Large enhancing mass at the rt pterygopalatine fossa (widened), sphenopalatine foramen (asterisk), nasal cavity extension
Anterior displacement of the posterior maxillary sinus wall
Extension into the sphenoid bone, sinus with sphenoid body erosion

15

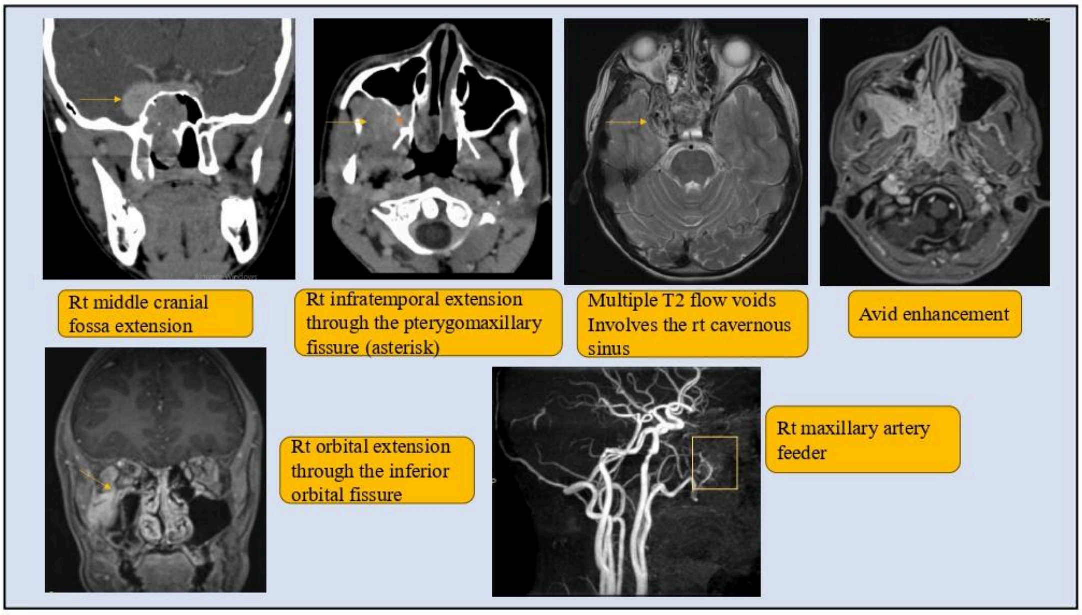
Rt middle cranial fossa extension
Rt infratemporal extension through the pterygomaxillary fissure (asterisk)
Multiple T2 flow voids Involves the rt cavernous sinus
Avid enhancement
Rt orbital extension through the inferior orbital fissure
Rt maxillary artery feeder

16

22nd Annual Scientific Meeting of Asian and Oceanic Society for Pediatric Radiology (AOSPR) 2024

Case 6

Juvenile angiofibroma

Highly vascular tumour
Posterior nasal cavity and nasopharynx
Locally aggressive
Tends to recur
Arises from the pterygopalatine fossa

Almost all are adolescent males
Presentation: nasal obstruction, epistaxis

CT + MRI
CT: useful for assessment of bone erosion and extension into sphenoid
Nasal cavity mass + pterygopalatine fossa + bone erosion behind the sphenopalatine foramen = JA
MRI: flow voids, enhancement ++ (very vascular)

Endoscopic surgical resection +/- RT, pre-op embolization

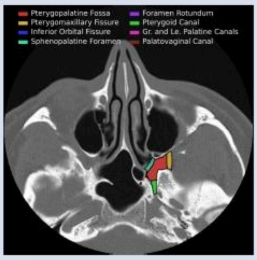

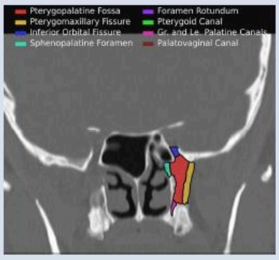

Case courtesy of Reuben Schmidt, Radiopaedia.org, rID: 177576

17

Key points

- Look for restricted diffusion -it can guide diagnosis
- Look at the extent of the tumour- it can insinuate (thin slice volumetric images are useful)
- Consider primary tumour or metastasis (in a young children with a lesion centred at bone always screen the abdomen for neuroblastoma)
- If multifocal tumours, think of an underlying genetic cancer predisposition syndrome
- Also consider differentials such as abscess (think of TB in our population)

18

Conclusion

Imaging plays a key role in diagnosis and follow-up of pediatric head and neck masses

Recognizing the imaging characteristics will improve diagnostic confidence and facilitate prompt diagnosis and management of malignant tumours

19

References

1. Lonergan GJ, Schwab CM, Suarez ES, Carlson CL. From the archives of the AFIP: neuroblastoma, ganglioneuroblastoma, and ganglioneuroma: radiologic-pathologic correlation. Radiographics. 2002 Jul;22(4):911-34.
2. Csanády M, Vass G, Bartyik K, Majoros V, Rovó L. Multidisciplinary management of cervical neuroblastoma in infants. International journal of pediatric otorhinolaryngology. 2014 Dec 1;78(12):2103-6.
3. Haddad M, Triglia JM, Helardot P, Couanet D, Gauthier F, Neuenschwander S, Bourlière B, Bergeron C, Munzer C, Rubie H, Guys JM. Localized cervical neuroblastoma: prevention of surgical complications. International journal of pediatric otorhinolaryngology. 2003 Dec 1;67(12):1361-7.
4. Biko DM, Anupindi SA, Hernandez A, Kersun L, Bellah R. Childhood Burkitt lymphoma: abdominal and pelvic imaging findings. American Journal of Roentgenology. 2009 May;192(5):1304-15.
5. Derinkuyu BE, Boyunağa Ö, Öztunalı Ç, Tekkeşin F, Damar Ç, Alımlı AG, Okur A. Imaging features of Burkitt lymphoma in pediatric patients. Diagnostic and Interventional Radiology. 2016 Jan;22(1):95
6. Lloyd C, McHugh K. The role of radiology in head and neck tumours in children. Cancer Imaging. 2010;10(1):49.
7. The Radiology Assistant. https://radiologyassistant.nl/head-neck/neck-masses/neck-masses-in-children#introduction-diagnostic-approach

20

21

Preventing Thermal Injury in Percutaneous Image-guided Ablation in Children - How Useful are Thermo-protective Strategies? A 5-year Retrospective Review

Way Loon Jonathan CHEN[1], Kin Fen Kevin FUNG[1], Hing Yan Danny CHO[2], Elaine Kan[1]

[1] *Department of Radiology, Hong Kong Children's Hospital, Hong Kong*
[2] *Department of Diagnostic and Interventional Radiology, Kwong Wah Hospital, Hong Kong SAR*

22nd Annual Scientific Meeting of Asian and Oceanic Society for Pediatric Radiology

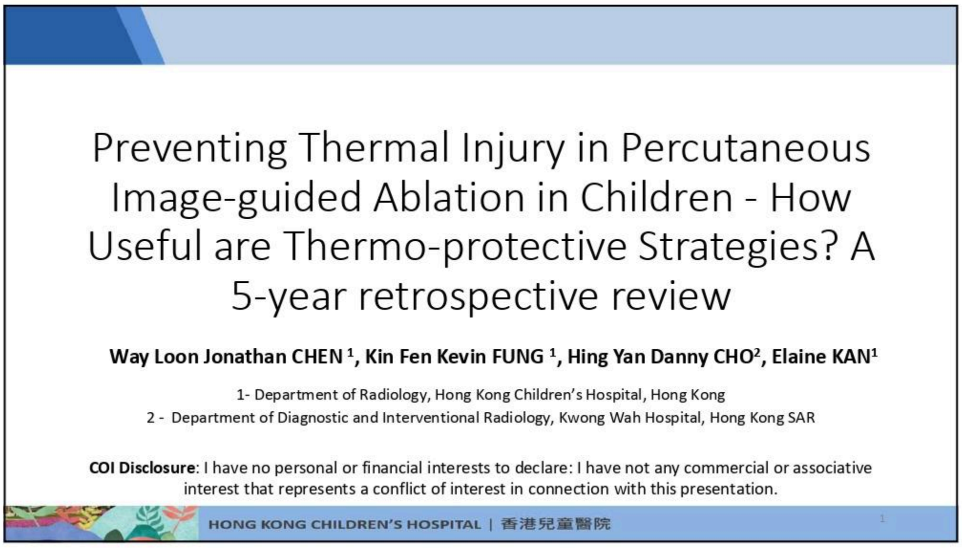

1

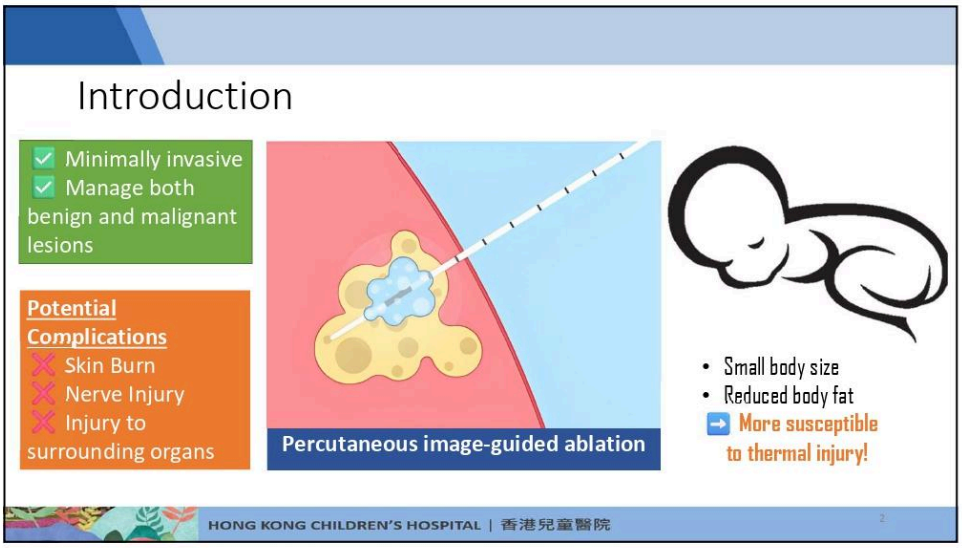

2

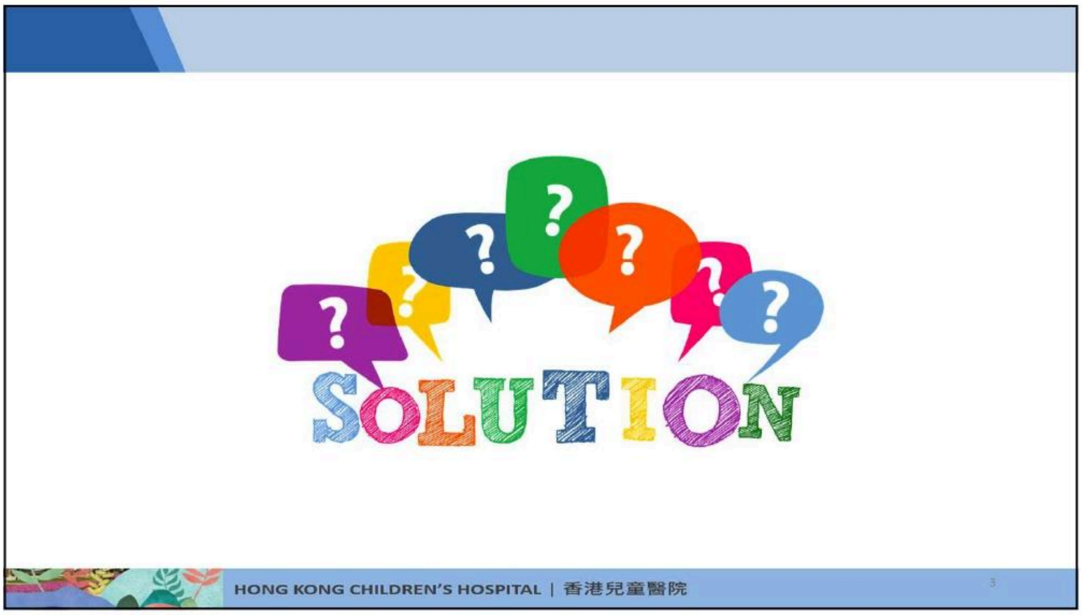
SOLUTION
HONG KONG CHILDREN'S HOSPITAL | 香港兒童醫院

3

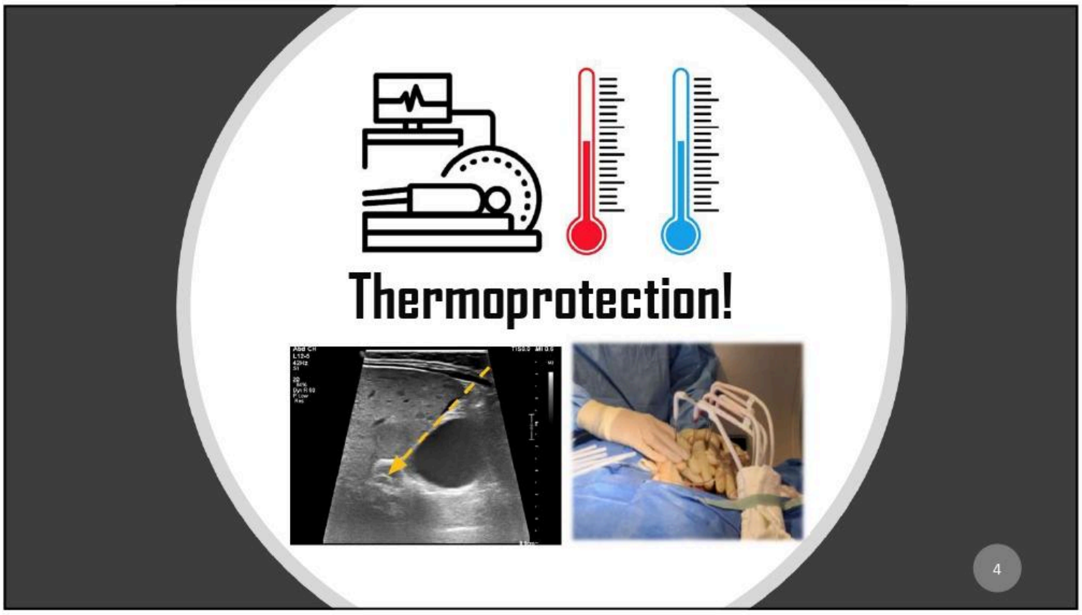
Thermoprotection!
4

4

Passive Thermoprotection: Neurophysiological Monitoring

- Under supervision of **on-site neurophysiologist**.
- **Continuous monitoring throughout procedure**.
- **Termination of freezing** (for cryoablation) following **significant SEP** and/or **MEP amplitude drop**.

5

Passive Thermoprotection: Temperature Monitoring

- **Intermittent screening** with **infra-red temperature gun**.
- **Real-time image monitoring** of **iceball / ablation zone**.

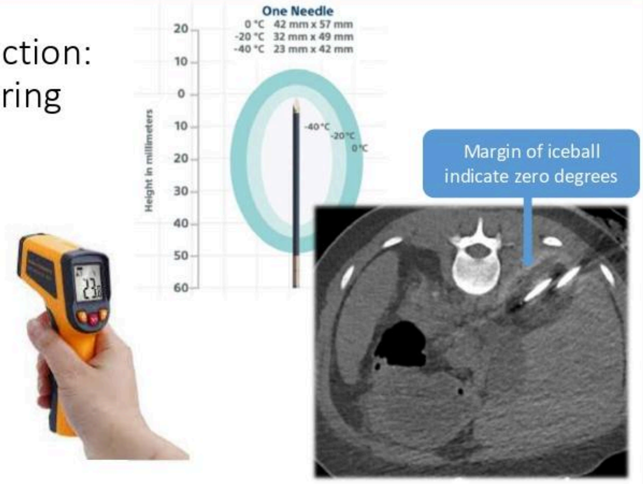

6

Active Thermoprotection

- **Hydrodissection** of **skin** & **fascial space**
- Creation of **artificial effusions**
- **Direct blunt needle displacement** of **intra-abdominal organs**

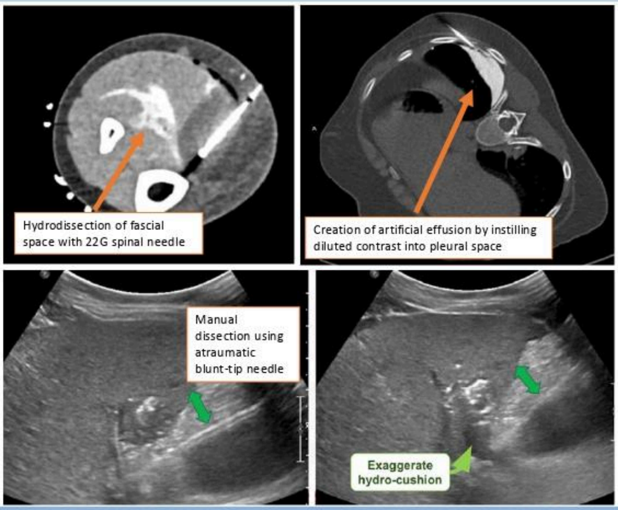

HONG KONG CHILDREN'S HOSPITAL | 香港兒童醫院

7

Active Thermoprotection (cont.)

- **Warm gloves** applied to skin surface.

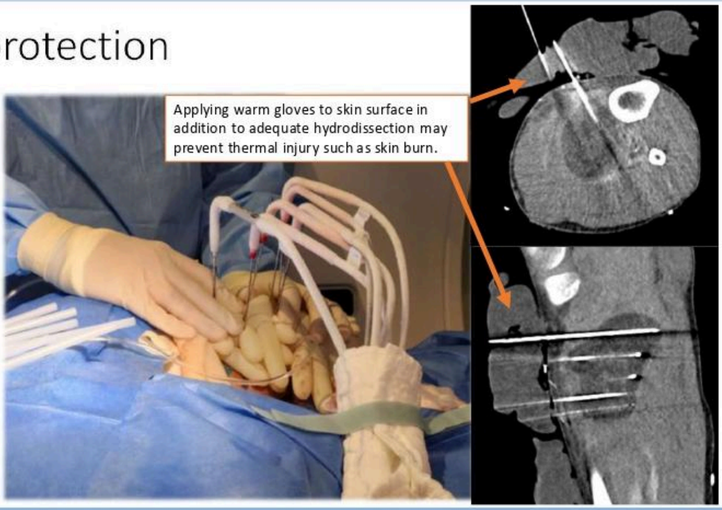

HONG KONG CHILDREN'S HOSPITAL | 香港兒童醫院

8

Purpose

To evaluate the utility of **thermo-protective measures** in **preventing thermal injury during ablation** in the **paediatric population**.

HONG KONG CHILDREN'S HOSPITAL | 香港兒童醫院

9

9

Materials and Methods

- **Retrospective** review.
- All patients undergoing image-guided percutaneous ablation of soft tissue lesions at our tertiary children's hospital from **June 2019** to **June 2024**.
- All patients underwent cross-sectional imaging with CT or MRI prior to, and after the procedure.

HONG KONG CHILDREN'S HOSPITAL | 香港兒童醫院

10

10

Materials and Methods

Parameters assessed:

- **Indications for image-guided percutaneous ablation**: included both neoplastic and non-neoplastic conditions for which ablation was performed either as a definitive or palliative therapy.
- **Modality of percutaneous ablation**.
- **Lesion characteristics**: ie location, size, volume, proximity to adjacent structures / organs.
- **Thermoprotective strategies deployed**: ie active vs passive.
- **Complications**.
- **Clinical Outcomes.**

HONG KONG CHILDREN'S HOSPITAL | 香港兒童醫院 11

11

Results

Lesion number	Location	Pathology	Volume (cm^3)	Type of Ablation	Complications (Y/N)
1	Posterior Rib	Osteosarcoma	4.3	Cryoablation	N
2	Anterior Rib	Osteosarcoma	5.6	Cryoablation	N
3	Left Calf	Desmoid tumour	270.6	Microwave Ablation	N
4	Kidney	Indeterminate renal lesion	8.5	Cryoablation	N
5	Liver	Hepatic Adenoma	14.7	Microwave Ablation	N
6	Liver	Hepatic Adenoma	8.0	Microwave Ablation	N
7	Liver	Hepatic Adenoma	8.0	Microwave Ablation	N
8	Liver	Hepatic Adenoma	8.0	Microwave Ablation	N
9	Liver	Hepatic Adenoma	4.0	Microwave Ablation	N
10	Liver	Hepatic Adenoma	6.2	Microwave Ablation	N
11	Liver	HCC	8.6	Microwave Ablation	N
12	Liver	HCC	11.3	Microwave Ablation	N
13	Supraclavicular fossa	Desmoid tumour	215.0	Cryoablation	Y
14	Left Calf	Desmoid Tumour	484.7	Cryoablation	Y

HONG KONG CHILDREN'S HOSPITAL | 香港兒童醫院 12

12

Results

14 lesions in 8 patients

Microwave Ablation	**Cryoablation**
8 lesions: All hepatic lesions.	6 lesions: MSK & Renal lesions.

- **Mean target lesion volume 75.5 cm^3** (range = 4.3 to 484.7 cm^3, and standard deviation = 145.5 cm3).
- **No complications observed** in **85.7%** of lesions (12/14).

13

Patient 1: Left Supraclavicular Desmoid Fibromatosis

Locally invasive - Encases left Subclavian artery & left Brachial plexus

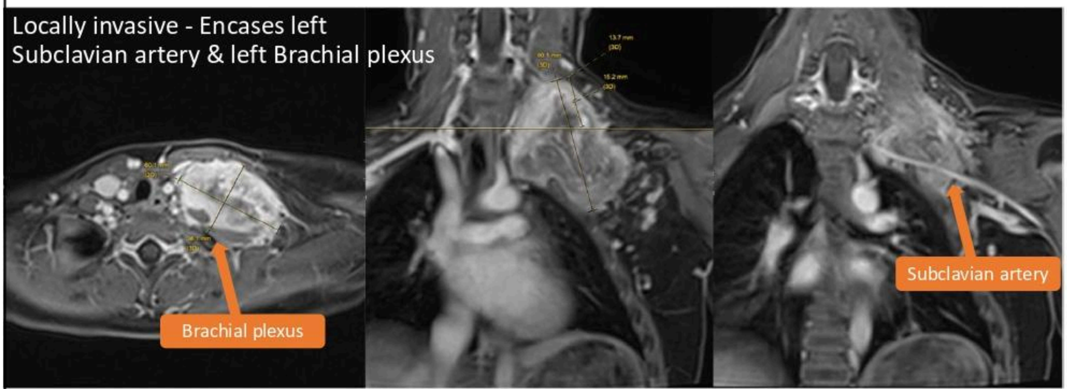

14

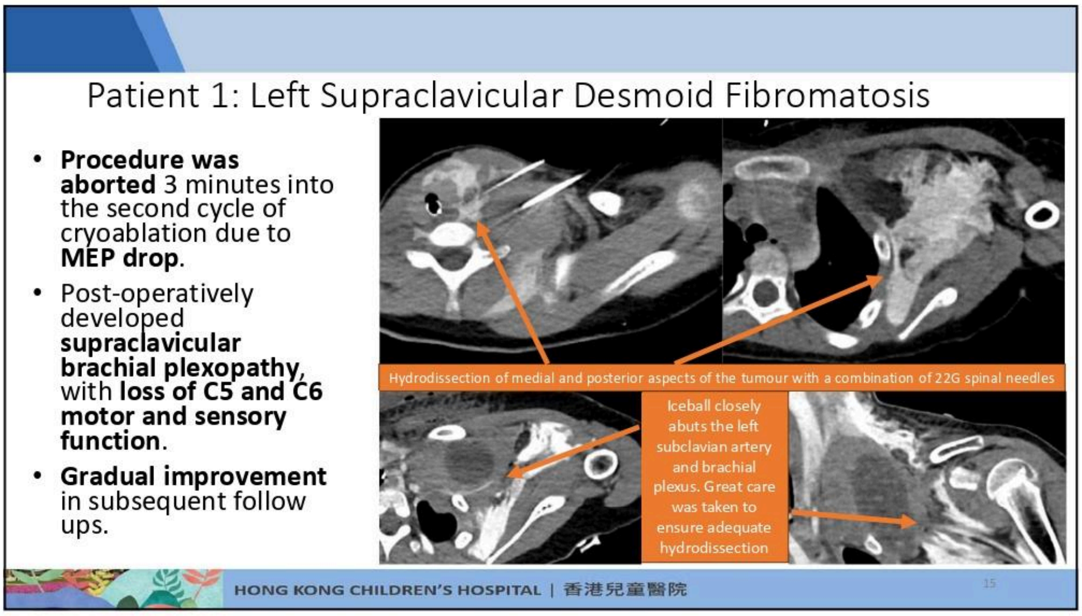
Patient 1: Left Supraclavicular Desmoid Fibromatosis
• Procedure was aborted 3 minutes into the second cycle of cryoablation due to MEP drop.
• Post-operatively developed supraclavicular brachial plexopathy, with loss of C5 and C6 motor and sensory function.
• Gradual improvement in subsequent follow ups.
Hydrodissection of medial and posterior aspects of the tumour with a combination of 22G spinal needles
Iceball closely abuts the left subclavian artery and brachial plexus. Great care was taken to ensure adequate hydrodissection
HONG KONG CHILDREN'S HOSPITAL | 香港兒童醫院
15

15

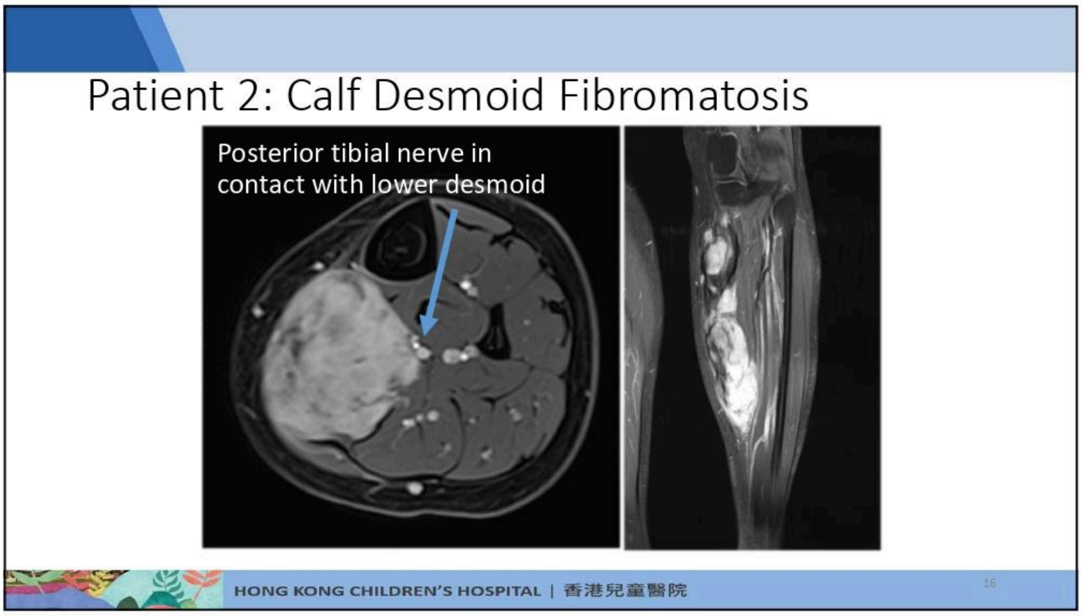
Patient 2: Calf Desmoid Fibromatosis
Posterior tibial nerve in contact with lower desmoid
HONG KONG CHILDREN'S HOSPITAL | 香港兒童醫院
16

16

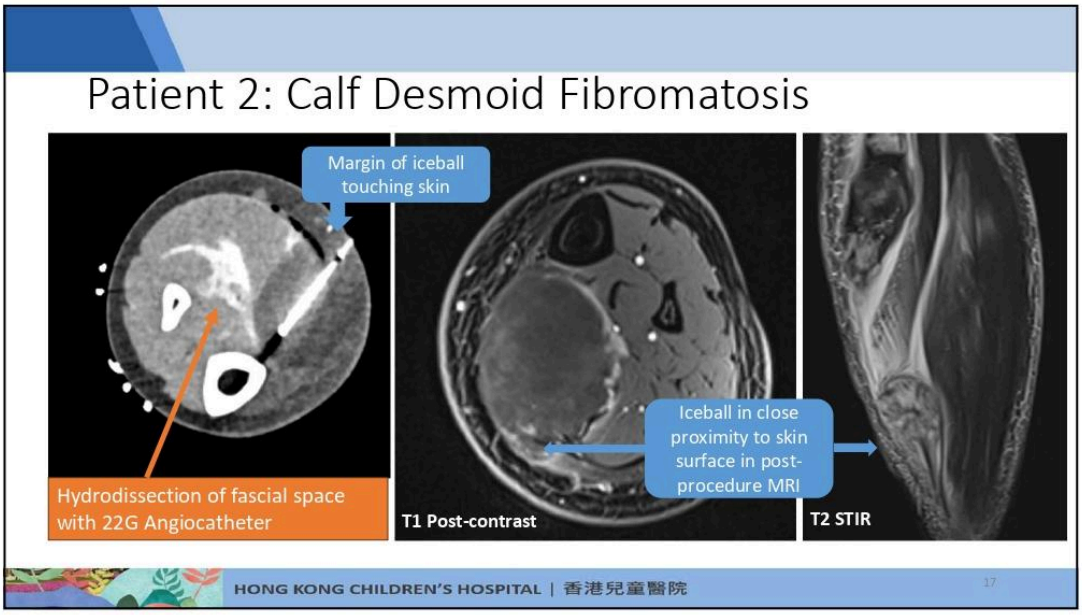
Patient 2: Calf Desmoid Fibromatosis
Margin of iceball touching skin
Hydrodissection of fascial space with 22G Angiocatheter
T1 Post-contrast
Iceball in close proximity to skin surface in post-procedure MRI
T2 STIR
HONG KONG CHILDREN'S HOSPITAL | 香港兒童醫院
17

17


Patient 2: Calf Desmoid Fibromatosis
• 2nd degree burn, complicated with Methicillin-sensitive Staphylococcus aureus wound infection.
• Attributed to inadequate coverage of skin with warm gloves and suboptimal visualisation of iceball in subcutaneous fat.
1 hour
3 hours
1 week
Fully healed, ~1 month post procedure
HONG KONG CHILDREN'S HOSPITAL | 香港兒童醫院
18

18

Discussion

- **Thermoprotective strategies** were **generally effective** in **preventing thermal injury related complications**.
- **Complications** were observed in lesions with **larger tumour volume** and those which **tumour debulking** was the treatment goal (vs total removal).

Limitations

- **Small cohort**.
- **Heterogeneous spectrum of lesions**.
- **Confounding factors**.

HONG KONG CHILDREN'S HOSPITAL | 香港兒童醫院 19

19

Key Takeaways

- **Careful pre-operative planning** for **optimal ablation zone size**.
- **Utilization of the various thermoprotection techniques** on a case-by-case basis.
- **Visualisation of ablation zone**: improves predictability of tumour coverage and prevents non-target ablation.

Coverage of skin with warm gloves

Complex lesions in close proximity to vital structures can pose challenges for hydrodissection

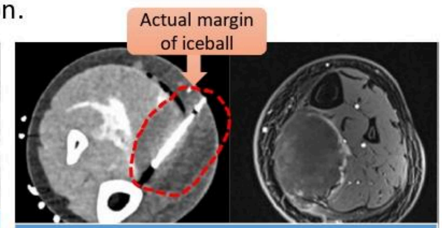

MRI is far superior to CT in terms of iceball visualization

HONG KONG CHILDREN'S HOSPITAL | 香港兒童醫院 20

20

References

1. Filippiadis DK, Binkert C, Pellerin O, Hoffmann RT, Krajina A, Pereira PL. Cirse Quality Assurance Document and Standards for Classification of Complications: The Cirse Classification System. CardioVascular and Interventional Radiology. 2017 Jun 5;40(8):1141–6.
2. Anil Nicholas Kurup, Morris JM, Boon AJ, Strommen JA, Schmit GD, Atwell TD, et al. Motor Evoked Potential Monitoring during Cryoablation of Musculoskeletal Tumors. Journal of Vascular and Interventional Radiology. 2014 Nov 1;25(11):1657–64.
3. Kumar Kempegowda Shashi, Shahin MM, Johnston P, Shaikh R. Cryoablation for Bone and Soft Tissue Lesions in Pediatric Patients: Complications and Preventive Measures. CardioVascular and Interventional Radiology. 2023 Aug 14;46(9):1249–56.
4. Alan Alper Sag, Husain AM. Thermal Protection Strategies and Neuromonitoring during Ablation. Seminars in Interventional Radiology. 2022 Apr 1;39(02):157–61.

HONG KONG CHILDREN'S HOSPITAL | 香港兒童醫院 21

21

22

Use of Multiparametric MRI in Evaluating Posterior Fossa Tumors in Pediatric Filipino Cohort

Kim Ivan R. Mendoza, Cyruz Jan B. David, Dan Philippe C. Nicer, Rovi Nino D. Samedra

Department of Radiology, University of the Philippines - Philippine General Hospital, Philippines

22nd Annual Scientific Meeting of Asian and Oceanic Society for Pediatric Radiology (AOSPR) 2024

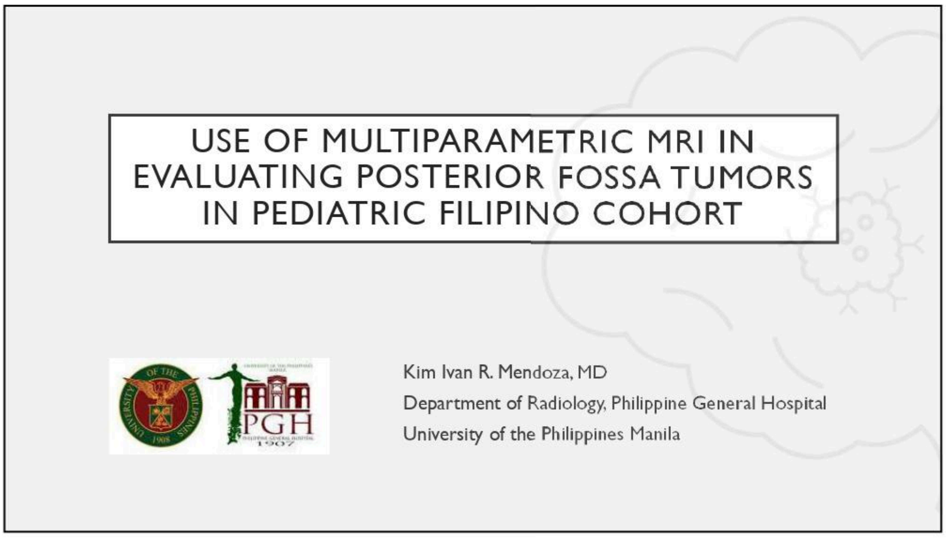

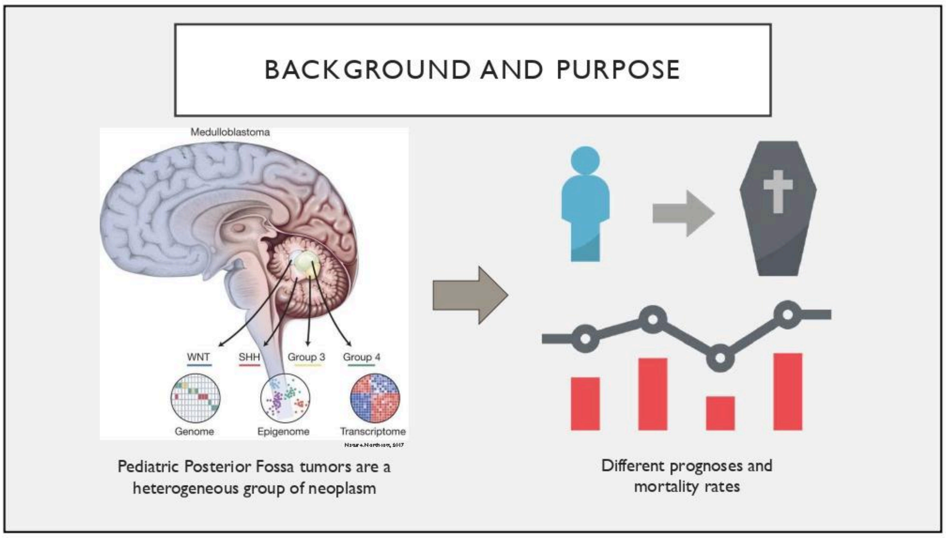

BACKGROUND AND PURPOSE

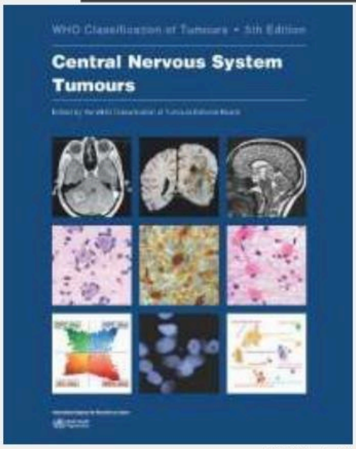

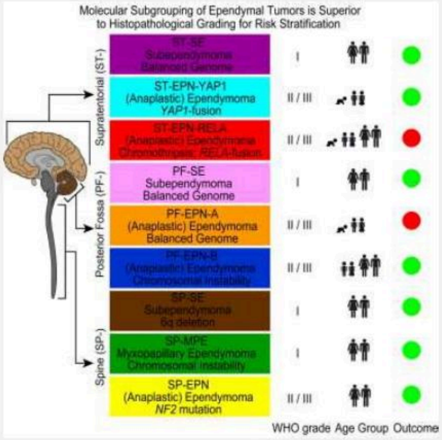

BACKGROUND AND PURPOSE

Challenges in low-middle-income countries like the Philippines

Difficult access to MRI; unrealized potential in LMICs

Resource-limited pathology departments

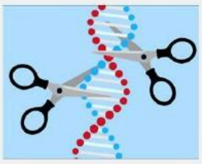

Poor access to genetic and molecular techniques

MATERIALS AND METHODS

A database search of radiologically diagnosed posterior fossa tumors

January 2022 to February 2024

Less than 18 years old

Complete preoperative MRI scan

Histopathologically diagnosed posterior fossa medulloblastoma, pilocytic astrocytoma, ependymoma, and AT/RT

Preoperative MRI review and diagnosis of number-coded patients by three histopathologically blinded radiologists using Alves et al. MR-based numeric flowchart

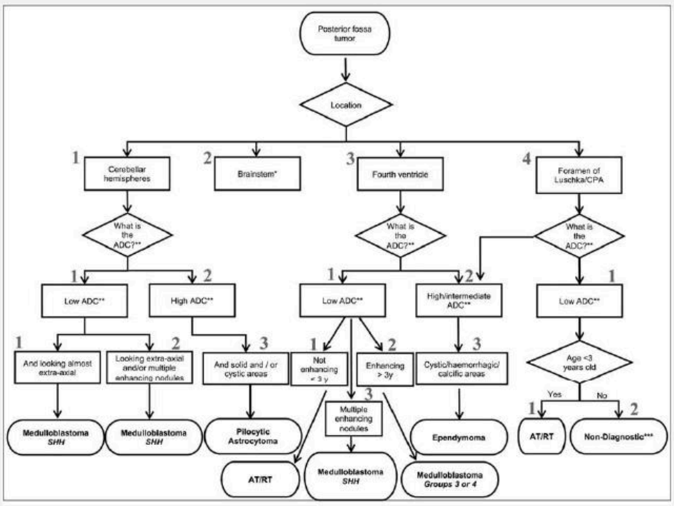

Figure 1. MR-based numeric flowchart from Alves et al 2021. Brainstem-arising tumors were excluded from the analysis and the ADC value/analysis was relative to gray matter.

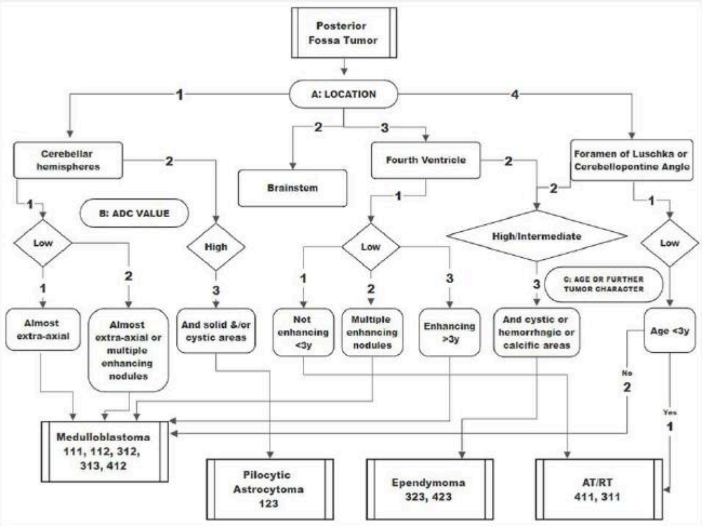

Figure 1. MR-based numeric flowchart adapted from Alves et al. Brainstem-arising tumors were excluded from the analysis and the ADC value/analysis was relative to gray matter.

RESULTS

Table 1. Clinicodemographic Characteristics of the Study Population

Characteristic	Overall	Medulloblastoma (N=25, 54.35%)	Pilocytic Astrocytoma (N=10, 21.74%)	Ependymoma (N=10, 21.74%)	AT/RT (N=1, 2.17%)
Age	7 (3–10)	7 (3–10)	8 (3–13)	5.5 (2–8)	0.67
Female	17 (36.96)	5 (20.00)	6 (60.00)	5 (50.00)	1 (100.00)
Location					
4th ventricle	29 (63.04)	21 (84.00)	2 (20.00)	5 (50.00)	1 (100.00)
Cerebellar vermis	3 (6.52)	0	3 (30.00)	0	0
Left CPA	4 (8.70)	1 (4.00)	0	3 (30.00)	0
Left Cerebellum	2 (4.35)	1 (4.00)	0	1 (10.00)	0
Right CPA	1 (2.17)	0	0	1 (10.00)	0
Right Cerebellum	7 (15.22)	2 (8.00)	5 (50.00)	0	0

Characteristic	Overall	Medulloblastoma (N=25, 54.35%)	Pilocytic Astrocytoma (N=10, 21.74%)	Ependymoma (N=10, 21.74%)	AT/RT (N=1, 2.17%)
T2 CHARACTER					
Cystic	8 (17.39)	0	8 (80.00)	0	0
Solid	10 (21.74)	10 (40.00)	0	0	0
Solid with hemorrhage	1 (2.17)	0	0	0	1 (100.00)
Solid with large cysts	13 (28.26)	7 (28.00)	2 (20.00)	4 (40.00)	0
Solid with large cysts & necrosis	1 (2.17)	0	0	1 (10.00)	0
Solid with necrosis	1 (2.17)	1 (4.00)	0	0	0
Solid with small cysts	12 (26.09)	7 (28.00)	0	5 (50.00)	0
Enhancement					
None	4 (8.70)	3 (12.00)	1 (10.00)	0	0
Present	28 (60.87)	14 (56.00)	6 (60.00)	8 (80.00)	0
Present (nodular)	14 (30.43)	8 (32.00)	3 (30.00)	2 (20.00)	1 (100.00)
ADC Value	750.625 (608–1086)	**633 (583.75–705.25)**	**1536.875 (1363.75–1786.25)**	1021.625 (873.75–1086)	639.5

Table 2. Statistical Analysis of MR-based numeric flowchart to discriminate posterior fossa tumors

Histopathologic diagnosis	TP	FP	FN	TN	Sn (%)	Sp (%)	PPV (%)	NPV (%)	LR+	LR-
Medulloblastoma	24	1	1	20	**96.00**	**95.24**	96.00	95.24	**20.16**	0.0420
Pilocytic Astrocytoma	7	1	3	35	70.00	**97.22**	87.50	92.11	**25.20**	0.3086
Ependymoma	9	4	1	32	90.00	88.89	69.23	**96.97**	8.10	0.1125
AT/RT	0	0	1	45	0	100.0	-	97.83	-	1.0000

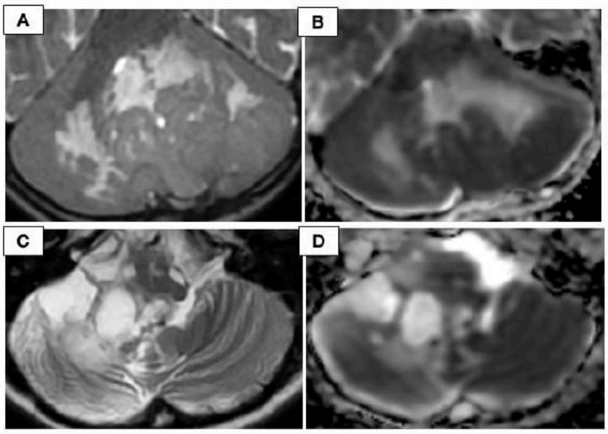

Figure 1. Differentials in pediatric posterior fossa masses centered in the cerebellar parenchyma. Axial T2WI (A) and ADC map (B) under pathway 1, with numeric flowchart of 112 suggesting medulloblastoma (histopathologically confirmed). Note the very low ADC values, presence of internal cysts, and large tumor infiltrating the left cerebellar parenchyma and vermis, all compatible with an embryonal tumor. Axial T2WI (C) and ADC map (D) under a similar pathway but with a numeric flowchart of 123, suggesting pilocytic astrocytoma (histopathologically confirmed). Notice the high ADC values and predominantly cystic appearance despite large tumor size and infiltration of the right cerebellar parenchyma.

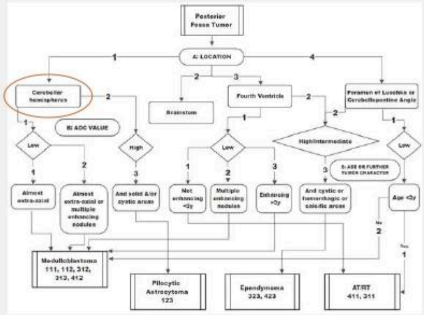

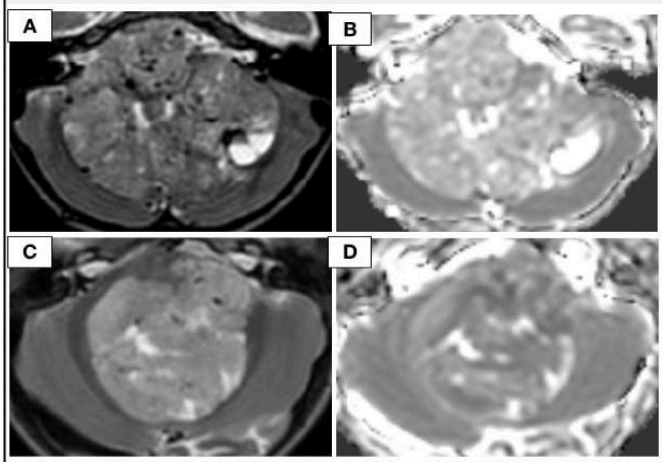

Figure 2. Differentials in pediatric posterior fossa masses centered in the fourth ventricle. Axial T2WI (A) and ADC map (B) under pathway 3, with numeric flowchart of 323 also suggesting ependymoma (histopathologically confirmed). Note the intermediate to high ADC despite large tumor size and internal vascularity, as well as presence of peripheral cysts. Axial T2WI (C) and ADC map (D) under a similar pathway but with numeric flowchart of 312, suggesting medulloblastoma (histopathologically confirmed). Notice the low ADC values and presence of internal cysts and vascularity, all suggestive of embryonal tumor.

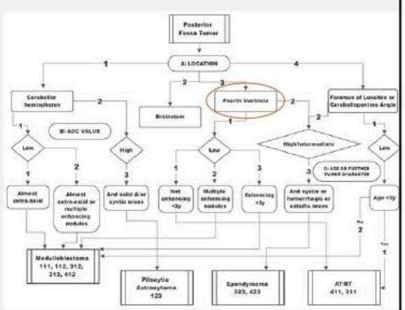

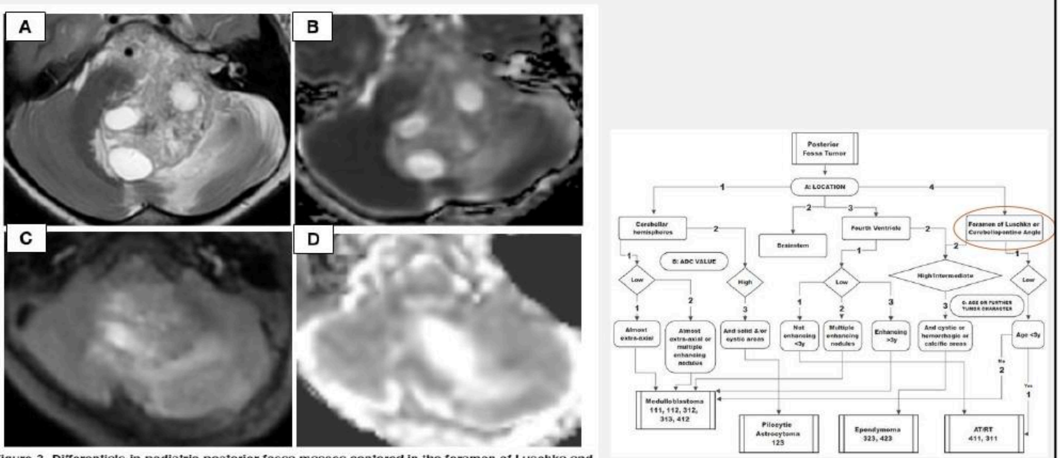

Figure 3. Differentials in pediatric posterior fossa masses centered in the foramen of Luschka and cerebellopontine angle. Axial T2WI (A) and ADC map (B) under pathway 4, with numeric flowchart of 423 suggesting ependymoma (histopathologically confirmed). Note the intermediate to high ADC and presence of cysts. Axial T2WI (C) and ADC map (D) under similar pathway but with numeric flowchart of 411 in a 5 month old child. In contrast to the other, note the low ADC values and similar presence of cysts. This only AT/RT patient was difficult to diagnose using the pathway as all radiologists centered the lesion in the fourth ventricle and noticed tumor enhancement (due to hemorrhage), thus calling a 312/313 sequence.

Table 3. Inter-rater Reliability of Pathways and Diagnoses Determined by the General Radiologist or the Resident Radiologist and the Neuroradiologist

Histopathologic diagnosis	According to numeric pathway			
	General radiologist		Resident radiologist	
	Agreement (%)	Kappa	Agreement (%)	Kappa
Overall	82.61	0.7881	80.43	0.7590
Medulloblastoma	76.00	0.6637	76.00	0.6495
Pilocytic Astrocytoma	90.00	0.7826	90.00	0.7826
Ependymoma	100.00	1.0000	80.00	0.6875

LIMITATIONS

- The study has some challenges, the main one being its **retrospective** nature. During image analysis, possible biases were controlled by **blinding** the MR interpreters with histopathologic diagnosis and **strict adherence** to the numeric-based flowchart.
- Another limitation of this study is its **small sample size** and **only one patient with AT/RT diagnosis**, which accounts for our confidence intervals and inability to calculate the diagnostic accuracy of pathway 311/411.
- Furthermore, the institution's **inability to classify medulloblastoma** into its **molecular subgroup** is a major limitation of this research, in contrast to the successful demonstration by the group of Alves et al.

IN SUMMARY

- This paper is the **first-largest cohort studying Filipino pediatric posterior fossa tumors**.
- **Medulloblastoma** is the most common pediatric posterior fossa tumor in our cohort
- The use of an MRI-based numeric pathway taking into account **age**, **location**, **tumor character**, and **ADC values** is diagnostically accurate in predicting histopathologic diagnosis, and possibly molecular subtype.
- This pathway is **easy to replicate** among neuroradiologists, general radiologists, and trainees, with substantial to near-perfect agreement.
- This stresses the importance of **adequate preoperative MRI evaluation** in our patients, as radiology can help **augment** the **resource-limited pathologic capabilities** of LMICs like the Philippines.

FURTHER DIRECTIONS

- **Collaboration** with other institutions can be done to produce a larger, more consistent analysis with an **increased sample size**, preferably using a **prospective** study design.
- Having a numeric flowchart that is validated and accurate can lead to the use of **radiogenomics** and **artificial intelligence applications**, now emerging fields in pediatric neuro-oncology.

REFERENCES

- Northcott PA, Buchhalter I, Morrissy AS, Hovestadt V, Weischenfeldt J, Ehrenberger T, et al. The whole-genome landscape of medulloblastoma subtypes. Nature. 2017 Jul;547(7663):311–7.
- Pajtler KW, Witt H, Sill M, Jones DT, Hovestadt V, Kratochwil F, Wani K, et. al. Molecular Classification of Ependymal Tumors across All CNS Compartments, Histopathological Grades, and Age Groups. Cancer Cell. 2015 May 11;27(5):728-43.
- Louis DN, Perry A, Wesseling P, Brat DJ, Cree IA, Figarella-Branger D, et al. The 2021 WHO Classification of Tumors of the Central Nervous System: a summary. Neuro-Oncology. 2021 Jun 29;23(8).
- Alves C a. PF, Löbel U, Martin-Saavedra JS, Toescu S, Tsunemi MH, Teixeira SR, et al. A Diagnostic Algorithm for Posterior Fossa Tumors in Children: A Validation Study. AJNR American journal of neuroradiology. 2021 May 1;42(5):961–8.
- Hanzlik E, Woodrome SE, Abdel-Baki M, Geller TJ, Elbabaa SK. A systematic review of neuropsychological outcomes following posterior fossa tumor surgery in children. Child's Nervous System. 2015 Sep 9;31(10):1869–75.
- Orduña P, Cheryl Anne Lubaton-Sacro. Factors associated with delayed diagnosis among Filipino pediatric brain tumor patients: a retrospective review. CNS oncology. 2022 Jun 9;11(3).

THANK YOU FOR YOUR KIND ATTENTION

For the Filipino children and every kid in the world battling and standing tall against all odds.

Confidence level	95%
Population Propotion	0.42
Marginal Error	0.08
Population Size	61
Alpha divided by 2	0.025
Z-score	1.959963985
Numerator	146.2155264
Denominator	3.396975842
n (sample)	**43.0428514**

Risk of Acute Kidney Injury After Contrast-enhanced MRI Examinations In A Pediatric Population

Hana Jeong[1], Pyeong Hwa Kim[1], Ah Young Jung[1], Jin Seong Lee[1], Young Ah Cho[1], Chong Hyun Suh[1], Jiwon Jung[2], Hee Mang Yoon[1]

1 Department of Radiology and Research Institute of Radiology, University of Ulsan College of Medicine, Republic of Korea
2 Department of Pediatrics, Asan Medical Center, University of Ulsan College of Medicine, Seoul, Republic of Korea

22nd Annual Scientific Meeting of Asian and Oceanic Society for Pediatric Radiology (AOSPR) 2024

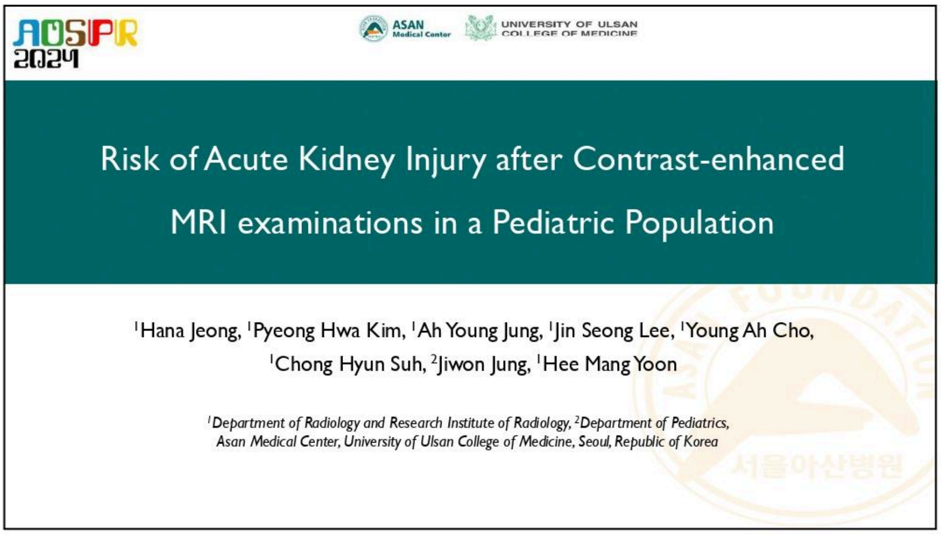

1

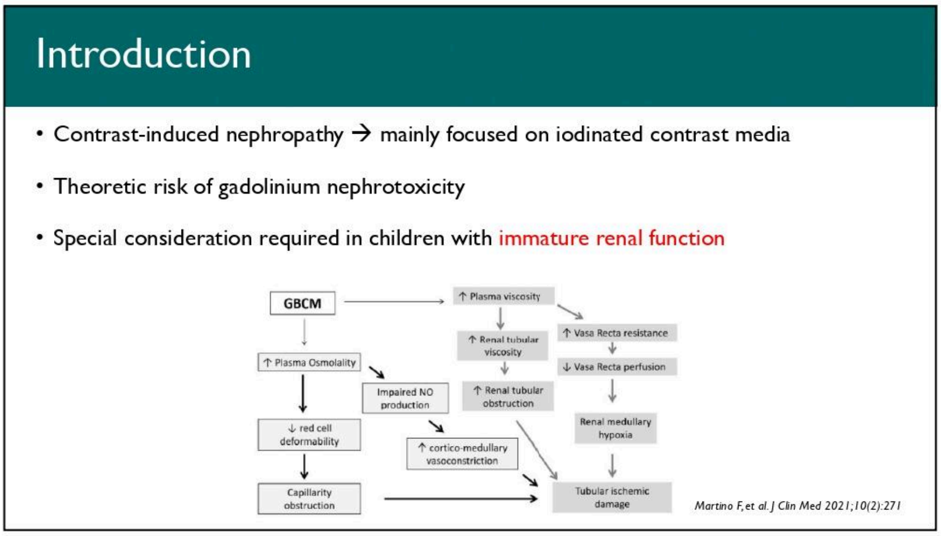

2

Purpose

To investigate the associations between GBCA administration and the occurrence of AKI in pediatric patients, and to determine the risks associated with AKI

3

Materials and Methods

4

Patients

- Single center, retrospective cohort study
- Consecutive pediatric patients (≤ 18 years) who underwent contrast-enhanced or unenhanced MRI between January 2015 ~ June 2021
- Exclusion
  - Unavailable height, weight, or serum creatinine within 3 months before MRI
  - Unavailable serum creatinine within 2 days after MRI
  - GBCA not administered intravenously (e.g., MR lymphangiography)
  - Additional MRI examinations obtained in one sitting (e.g., consecutive brain → spine MRI in one slot)
    - Only the prior MRI examination included

5

Outcomes

Primary outcome

Occurrence of AKI

Enhanced vs. unenhanced MRI

- Serum creatinine ≥ 0.3 mg/dL or 50% within 48 hours after MRI

K-DIGO guideline (Nephron Clin Pract 2012;120:c179-84)

Variables for propensity score estimation

- Age
- Examination type (CNS vs. non-CNS)
- Body mass index
- Calculated eGFR (bedside Schwartz calculation)
- CKD stage
- Diabetes mellitus
- Cardiovascular disease

Statistical analysis

① Per-examination basis Multivariable logistic regression analysis using generalized estimating equation (GEE)

② Propensity score matching (PSM)

③ Inverse probability of treatment weighting (IPTW) analysis

6

Statistical analysis

- Multivariable logistic regression using GEE to explore factors associated with AKI after MRI
- Propensity score analysis
  - Hosmer-Lemeshow test → discrimination for propensity score model
  - C-statistic → calibration for propensity score model
  - Standardized mean difference (SMD) > 0.1 → considered as imbalanced
- Subgroup analysis (age, sex, CKD stage, diabetes mellitus, cardiovascular disease)

7

Results

8

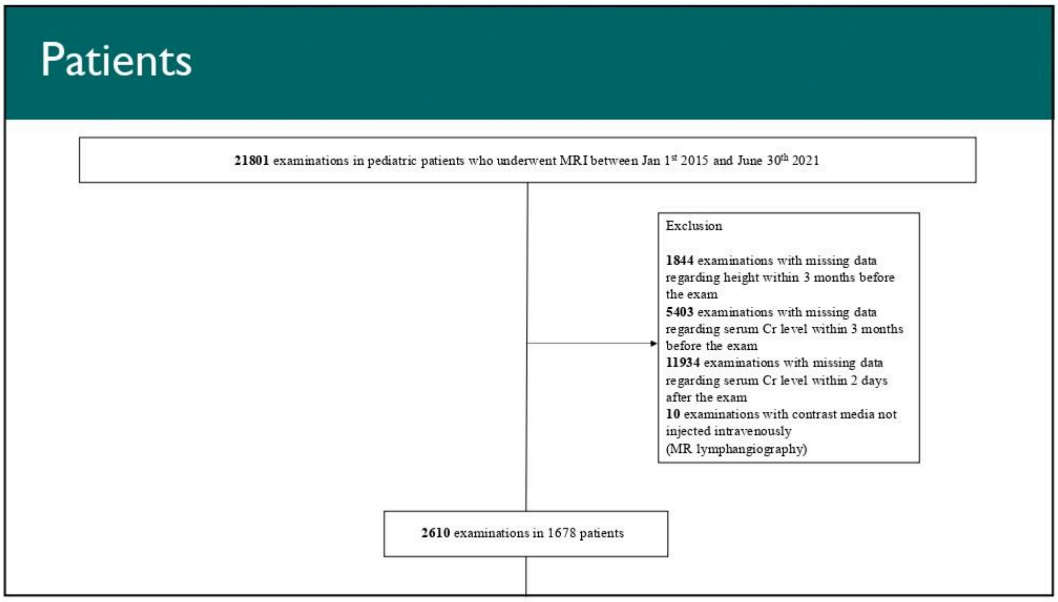
Patients
21801 examinations in pediatric patients who underwent MRI between Jan 1st 2015 and June 30th 2021
Exclusion
1844 examinations with missing data regarding height within 3 months before the exam
5403 examinations with missing data regarding serum Cr level within 3 months before the exam
11934 examinations with missing data regarding serum Cr level within 2 days after the exam
10 examinations with contrast media not injected intravenously (MR lymphangiography)
2610 examinations in 1678 patients

9

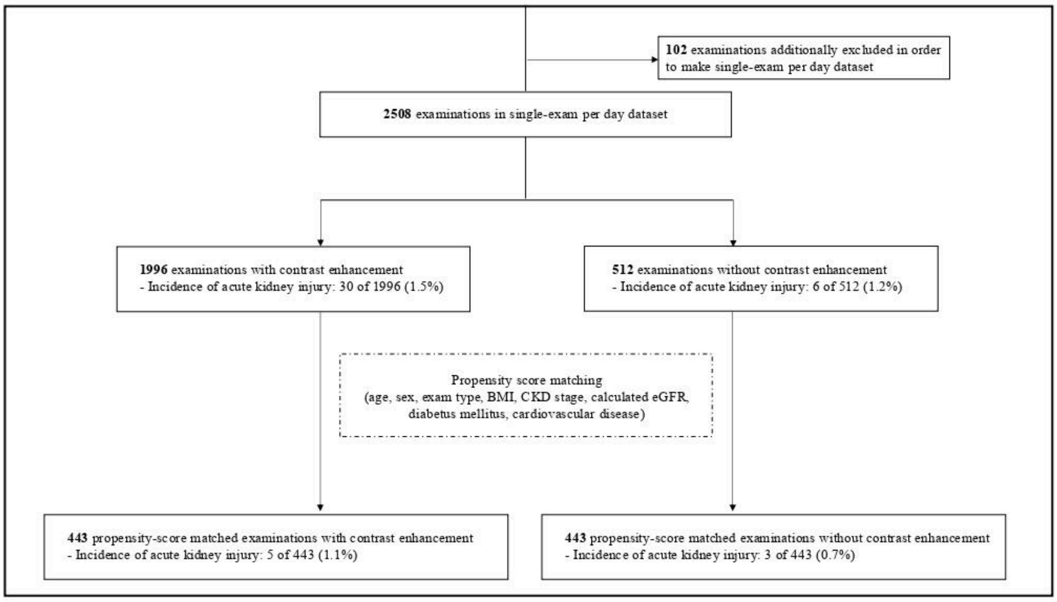
102 examinations additionally excluded in order to make single-exam per day dataset
2508 examinations in single-exam per day dataset
1996 examinations with contrast enhancement
- Incidence of acute kidney injury: 30 of 1996 (1.5%)
512 examinations without contrast enhancement
- Incidence of acute kidney injury: 6 of 512 (1.2%)
Propensity score matching
(age, sex, exam type, BMI, CKD stage, calculated eGFR, diabetus mellitus, cardiovascular disease)
443 propensity-score matched examinations with contrast enhancement
- Incidence of acute kidney injury: 5 of 443 (1.1%)
443 propensity-score matched examinations without contrast enhancement
- Incidence of acute kidney injury: 3 of 443 (0.7%)

10

22nd Annual Scientific Meeting of Asian and Oceanic Society for Pediatric Radiology (AOSPR) 2024

Baseline characteristics

	Total set (n=2508)			Propensity score matched set (n=886)			IPTW set (n=3378)		
Characteristic	Noncontrast group (n=512)	Contrast group (n=1996)	SMD	Noncontrast group (n=443)	Contrast group (n=443)	SMD	Noncontrast group (n=1706)	Contrast group (n=1672)	SMD
Mean age, years	9.0 ± 6.9	9.3 ± 6.2	0.06	9.0 ± 6.8	9.3 ± 6.3	0.05	9.2 ± 6.7	8.8 ± 6.4	0.06
Sex			0.15			0.01			0.08
Boys	241 (47.1)	1087 (54.5)		202 (45.6)	205 (46.3)		949 (55.6)	863 (51.6)	
Girls	271 (52.9)	909 (45.5)		241 (54.4)	238 (53.7)		757 (44.4)	809 (48.4)	
Exam type			0.38			0.12			0.06
Non-CNS	77 (15.0)	616 (30.9)		67 (15.1)	87 (19.6)		478 (28.0)	512 (30.6)	
CNS	435 (85.0)	1380 (69.1)		376 (84.9)	356 (80.4)		1228 (72.0)	1160 (69.4)	
Body mass index, kg/m²	18.17 (5.2)	18.56 (4.6)	0.08	18.2 (5.1)	18.4 (5.0)	0.05	18.8 (5.4)	18.4 (4.7)	0.08
CKD stage			0.38			0.15			0.06
1	333 (65.0)	1594 (79.9)		297 (67.0)	303 (68.4)		1228 (72.0)	1230 (73.6)	
2	101 (19.7)	278 (13.9)		86 (19.4)	94 (21.2)		315 (18.5)	282 (16.9)	
3	40 (7.8)	88 (4.4)		34 (7.7)	28 (6.3)		107 (6.3)	103 (6.2)	
4	24 (4.7)	29 (1.5)		18 (4.1)	16 (3.6)		39 (2.3)	46 (2.7)	
5	14 (2.7)	7 (0.4)		8 (1.8)	2 (0.5)		17 (1.0)	11 (0.7)	
Calculated eGFR, mL/min/1.73m²	100.3 ± 44.4	123.8 ± 48.6	0.51	100.9 ± 41.2	105.0 ± 39.8	0.10	116.8 ± 61.8	111.9 ± 42.9	0.09
Diabetes mellitus	7 (1.4)	41 (2.1)	0.05	5 (1.1)	7 (1.6)	0.04	32 (1.9)	27 (1.6)	0.02
Cardiovascular disease	33 (6.4)	162 (8.1)	0.06	26 (5.9)	23 (5.2)	0.03	130 (7.6)	111 (6.7)	0.04

Noncontrast group showed

- CNS (e.g., brain or spine) exam↑
- Renal insufficiency↑

→ Imbalanced in PSM, but balanced in IPTW

Acceptable

Calibration

Hosmer-Lemeshow P=0.40 (>0.05)

Discrimination

C-statistic=0.689

11

Risk of AKI

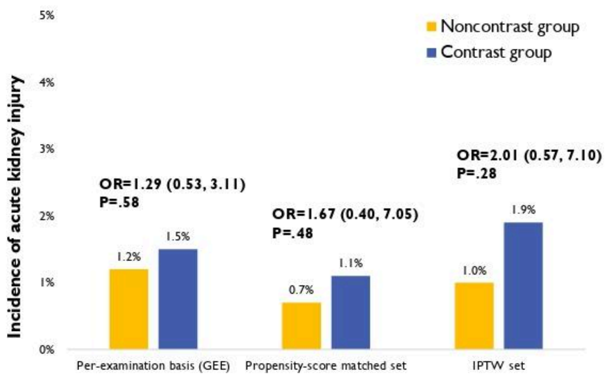

No significant difference of AKI

Enhanced vs. unenhanced MR

12

22nd Annual Scientific Meeting of Asian and Oceanic Society for Pediatric Radiology (AOSPR) 2024

Regression and subgroup analysis

Factors associated with AKI

Variable	OR (95% CI)	P-value
Age	0.94 (0.89–1.00)	0.051
Sex	Eliminated	
Examination type	Eliminated	
BMI	Eliminated	
CKD stage		
1	Reference category	
2	0.37 (0.09–1.54)	0.17
3	0.38 (0.05–3.00)	0.36
4	0.94 (0.12–7.29)	0.95
5	10.66 (3.15–36.09)	<0.001
Calculated eGFR	Eliminated	
Diabetes mellitus	3.63 (0.74–17.97)	0.11
Cardiovascular disease	Eliminated	

Subgroup analysis

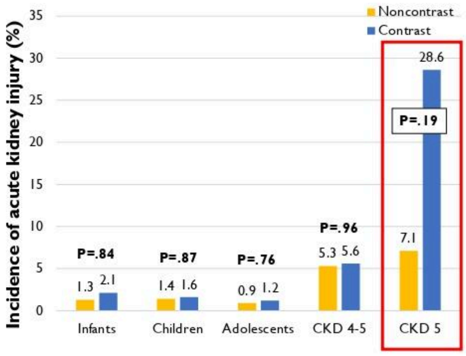

13

Limitation

- Sample size (especially neonates, CKD stage 5)
- Exclusively used gadoterate meglumine (97%)
- Urine output (one of AKI criteria) not considered
- Confounding variables (e.g., nephrotoxic drug or sepsis) not fully considered

14

Conclusion

- The incidence rate of acute kidney injury following contrast-enhanced MRI examinations was similar to that following unenhanced MRI examinations.

- Although there was no interaction between CKD stage and GBCA, numerically higher incidence of AKI in the contrast group with CKD stage 5 warrants careful interpretation.

15

Thank you for the attention!

Pyeong Hwa Kim, MD, PhD
phkim@amc.seoul.kr

Assistant professor

Department of Radiology and Research Institute of Radiology, Asan Medical Center, University of Ulsan College of Medicine, Korea

16